Conservation and divergence of UVR8-COP1/SPA-HY5 signaling in UV-B responses of *Marchantia polymorpha*

Yuanke Liang[1,l,#], Roman Podolec[1,¶,#], Richard Chappuis[1], Emmanuel Defossez[2], Gaétan Glauser[3], Johannes Rötzer[4,5], Sara Christina Stolze[6], Liam Dolan[4], Hirofumi Nakagami[6], Emilie Demarsy[1], Roman Ulm[1,7,*]

[1]Department of Plant Sciences, Section of Biology, Faculty of Sciences, University of Geneva, 1211 Geneva 4, Switzerland

[2]Institute of Biology, University of Neuchâtel, 2000 Neuchâtel, Switzerland

[3]Neuchâtel Platform of Analytical Chemistry, University of Neuchâtel, 2000 Neuchâtel, Switzerland

[4]Gregor Mendel Institute of Molecular Plant Biology (GMI), Austrian Academy of Sciences, 1030 Vienna, Austria

[5]Vienna BioCenter PhD Program, Doctoral School of the University of Vienna and Medical University of Vienna, 1030 Vienna, Austria

[6]Max-Planck Institute for Plant Breeding Research, D-50829, Cologne, Germany

[7]Institute of Genetics and Genomics of Geneva (iGE3), University of Geneva, 1211 Geneva 4, Switzerland

[l]Present address: Max-Planck-Institute of Molecular Plant Physiology, Potsdam-Golm, Germany

[¶]Present address: Whitehead Institute for Biomedical Research, Cambridge, MA, USA

[#]These authors contributed equally.

[*]Author for correspondence: roman.ulm@unige.ch (R.U.)

ABSTRACT

Ultraviolet-B radiation (UV-B) poses a major challenge to all forms of plant life. The liverwort *Marchantia polymorpha* (Marchantia) serves as a key model organism to study signaling pathways and to infer their evolution throughout the green lineage. Marchantia expresses key components of UV-B signaling, including the photoreceptor UV RESISTANCE LOCUS 8 (MpUVR8), the

WD40-repeat protein REPRESSOR OF UV-B PHOTOMORPHOGENESIS (MpRUP), the E3 ubiquitin ligase complex CONSTITUTIVELY PHOTOMORPHOGENIC 1 / SUPPRESSOR OF phyA-105 (MpCOP1/MpSPA), and the transcriptional regulator ELONGATED HYPOCOTYL 5 (MpHY5). Here, we show that MpUVR8 exists as a homodimer in its ground-state in vivo, then monomerizes and accumulates in the nucleus upon UV-B activation. Activated MpUVR8 interacts with MpCOP1, triggering growth inhibition, genome-wide gene expression changes, biosynthesis of UV-absorbing metabolites, and photoprotection, which overall contributes to UV-B stress tolerance. MpRUP facilitates redimerization of MpUVR8 and Mp*rup* null mutants show enhanced UV-B photomorphogenesis, demonstrating that MpRUP efficiently represses MpUVR8 signaling. Unlike the case in Arabidopsis and in contrast to the strong Mp*cop1* mutant phenotype, Mp*spa* mutants develop only a very weak constitutive photomorphogenesis phenotype, indicating that COP1 function is much more independent of SPA in Marchantia than in Arabidopsis. Moreover, in contrast to Arabidopsis SPAs, Mp*spa* is linked with a hyper-responsive UV-B phenotype, suggesting that MpSPA is a negative regulator of MpUVR8 signaling. Similar to Arabidopsis HY5/HYH, MpHY5 functions antagonistically to MpCOP1, but its role in UV-B-mediated gene expression changes is more limited. Our findings demonstrate that although core components of UV-B signaling existed in the last common ancestor of extant land plants, regulatory interactions have diversified in different lineages since their divergence more than 400 million years ago.

INTRODUCTION

Photoautotrophic plants have a “love/hate relationship” with light. Light is required for photosynthesis, but sunlight poses major challenges due to potentially damaging ultraviolet-B radiation (UV-B; 280–315 nm) (Demarsy et al., 2018). Plants have a unique and conserved UV-B photoreceptor UV RESISTANCE LOCUS 8 (UVR8) that is crucially important for UV-B acclimation, tolerance, and survival (Kliebenstein et al., 2002; Rizzini et al., 2011; Tilbrook et al., 2016; Li et al., 2018; Soriano et al., 2018; Rai et al., 2019; Podolec et al., 2021a; Hu et al., 2024; Stockenhuber et al., 2024). The UVR8 signaling pathway has mainly been outlined in Arabidopsis, with UVR8 being a homodimer in its ground state, which exhibits monomerization after absorption of UV-B photons by intrinsic tryptophan (Trp) residues, followed by accumulation in the nucleus (Kaiserli and Jenkins, 2007; Rizzini et al., 2011; Christie et al., 2012; Wu et al., 2012; Yin et al., 2016; Li et al., 2020; Qian et al., 2020; Podolec et al., 2021a; Fang et al., 2022). Activated UVR8

63 then interacts with CONSTITUTIVELY PHOTOMORPHOGENIC 1 (COP1) (Favory et al., 2009;
64 Yin et al., 2015; Wang et al., 2022). COP1 forms an E3 ubiquitin ligase complex together with
65 SUPPRESSOR OF phyA-105 proteins (SPA1–4 in Arabidopsis) (Laubinger et al., 2004; Chen et
66 al., 2010). The COP1/SPA complex represses photomorphogenesis by ubiquitinating
67 photomorphogenesis-promoting factors, directing them to degradation by the 26S proteasome
68 (Podolec and Ulm, 2018; Ponnu and Hoecker, 2021). UV-B-activated UVR8 inhibits the activity
69 of the COP1-SPA complex through a cooperative, high-affinity binding mechanism that displaces
70 substrate proteins from COP1, thus allowing the stabilization of key transcription factors, including
71 the basic leucine zipper (bZIP) transcriptional regulators ELONGATED HYPOCOTYL 5 (HY5)
72 and HY5 HOMOLOG (HYH) (Holm et al., 2002; Ulm et al., 2004; Oravecz et al., 2006; Binkert
73 et al., 2014; Lau et al., 2019). This ultimately leads to broad changes in gene expression upon UV-
74 B exposure (Brown et al., 2005; Favory et al., 2009; Tavridou et al., 2020b). COP1/SPA together
75 with HY5/HYH thus represents a major regulatory hub in light signaling in Arabidopsis (Holm et
76 al., 2002; Ulm et al., 2004; Ponnu et al., 2019). The two WD-40 repeat proteins REPRESSOR OF
77 UV-B PHOTOMORPHOGENESIS 1 (RUP1) and RUP2 act as negative feedback regulators of
78 the UVR8 photocycle by facilitating UVR8 redimerization, thereby repressing UV-B signaling
79 (Gruber et al., 2010; Heijde and Ulm, 2013; Podolec et al., 2021b; Wang et al., 2023).

80 The core components of UVR8 signaling seem to be evolutionarily conserved in the green
81 lineage, since they are present in the alga *Chlamydomonas reinhardtii* (hereafter Chlamydomonas)
82 (Allorent et al., 2016; Tilbrook et al., 2016; Tokutsu et al., 2019; Dannay et al., 2025) and the
83 liverwort *Marchantia polymorpha* (hereafter Marchantia) (Clayton et al., 2018; Soriano et al., 2018;
84 Kondou et al., 2019). Notably, Marchantia has minimal gene redundancy in many signaling
85 pathways, and many studies in the past decade have contributed to our understanding of the origins
86 and evolution of major plant regulatory pathways (Bowman et al., 2017; Liang et al., 2022;
87 Frangedakis et al., 2024). The Marchantia genome indeed possesses single homologs for genes
88 encoding UVR8 signaling-related components, such as MpUVR8, MpRUP, MpCOP1, MpSPA,
89 and MpHY5. Although a few studies have explored the role of some of these components in UV-
90 B (Clayton et al., 2018; Soriano et al., 2018; Kondou et al., 2019) and visible light signaling (Zhang
91 et al., 2021; Yelina et al., 2024), a deeper understanding of their activities and roles in UV-
92 acclimation is warranted to understand to what extent the molecular mechanisms by which these

93 components mediate UV acclimation and tolerance are conserved or divergent throughout the plant
94 kingdom.

95 We investigated if the major UVR8 signaling components have functionally diverged
96 during plant evolution, and how mechanisms underlying UV-B tolerance may have evolved during
97 the colonization of land by plants. We extend our understanding of the crucial role of MpUVR8 in
98 UV-B acclimation and survival in Marchantia, and provide unequivocal evidence clarifying
99 conservation of the UVR8 photocycle in Marchantia. However, although Mp*cop1* mutants
100 exhibited enhanced constitutive photomorphogenesis and extreme dwarfism comparable to UV-B-
101 grown Mp*rup* mutants, Mp*spa* mutants showed only a very weak constitutive photomorphogenesis
102 phenotype in visible light. Surprisingly however, Mp*spa* mutants were hyper-responsive to UV-B,
103 suggesting that MpSPA plays a divergent role from that in Arabidopsis. We further provide a
104 genome-wide view of MpUVR8-mediated transcriptional responses in Marchantia and identify
105 UV-B-regulated gene clusters and metabolites key to UV-B protection. Notably, different to
106 HY5/HYH being major regulators in Arabidopsis, our transcriptome data revealed that only a few
107 UV-B-regulated genes were entirely MpHY5-dependent.
108

109 RESULTS

110 MpUVR8 is homodimeric in its ground state, and monomerizes and accumulates in nuclei in 111 response to UV-B

112 In Marchantia, UVR8 is encoded by a single locus, but alternative splicing of the 11th intron
113 produces two transcripts, namely Mp*UVR8.1* and Mp*UVR8.2*, resulting in two different proteins
114 whereby residues 414 to 426 present in MpUVR8.1 are absent in MpUVR8.2 (fig. S1) (Soriano et
115 al., 2018). Whether MpUVR8 forms homodimers *in vivo* or is primarily monomeric with a
116 divergent inactivation mechanism is unclear (Soriano et al., 2018). We thus first tested if
117 MpUVR8.1 and MpUVR8.2 form dimers using a luciferase complementation imaging (LCI) assay
118 in transiently transformed *Nicotiana benthamiana* leaves (Zhou et al., 2018). Resulting LCI signals
119 showed interactions of MpUVR8.1 and MpUVR8.2 both with and between themselves, indicating
120 that MpUVR8 forms homodimers *in vivo* (Fig. 1A to C). In AtUVR8, the aspartate-96 (D96) and
121 aspartate-107 (D107) residues are key to homodimer formation and mutating each to asparagine
122 impairs UVR8^{D96N,D107N} dimer formation (Christie et al., 2012; Wu et al., 2012; Heilmann et al.,
123 2016; Podolec et al., 2021b). Consistent with the conservation of these residues in MpUVR8 (fig.

124 S1), no LCI signal was detected with the mutated MpUVR8.1^{D95N,D106N} and MpUVR8.2^{D95N,D106N}
125 variants (Fig. 1A and B).
126 To further test if endogenous MpUVR8 forms homodimers, we crosslinked protein extracts
127 from Marchantia with dithiobis (succinimidyl propionate) (DSP), as described previously for
128 Arabidopsis (Rizzini et al., 2011; Podolec et al., 2021b). Using a specific anti-MpUVR8 antibody,
129 we detected a band at the size of the predicted MpUVR8 dimer at about 100 kDa in the absence of
130 UV-B, and this band was strongly reduced in extracts from UV-B-treated plants (Fig. 1D). These
131 data indicate that UV-B exposure induces MpUVR8 monomerization. Of note, UV-B-activated
132 monomeric MpUVR8 was not well detected in crosslinked extracts, as in Arabidopsis (Rizzini et
133 al., 2011; Podolec et al., 2021b). However, we detected MpUVR8 at its monomeric size of about
134 48 kDa (predicted sizes for MpUVR8.1 and MpUVR8.2 are 48.6 and 47.1 kDa, respectively) both
135 following the reversal of DSP crosslinking with the reducing agent β-mercaptoethanol (β-ME) and
136 in the absence of crosslinking (Fig. 1D), demonstrating that MpUVR8 levels are not affected by
137 UV-B treatment or crosslinking.
138 To define MpUVR8 subcellular localization in Marchantia, we transformed wild-type Tak-
139 1 with the full genomic Mp*UVR8* locus containing an N-terminal green fluorescent protein (GFP)
140 tag and imaged the resulting fluorescence. GFP-MpUVR8 accumulated in the nucleus only when
141 plants were exposed to UV-B (Fig. 1E), similar to AtUVR8 (Kaiserli and Jenkins, 2007; Yin et al.,
142 2016) and the 35S promoter–driven expression of Citrine-MpUVR8 in Tak-1 (Kondou et al., 2019).
143 This contrasts with the apparent constitutive nuclear localization of GFP-MpUVR8.1 and GFP-
144 MpUVR8.2 when expressed in Arabidopsis and *N. benthamiana* (Soriano et al., 2018). We
145 conclude that upon UV-B exposure MpUVR8 monomerize and accumulate in nuclei in Marchantia.
146

147 ## MpRUP facilitates MpUVR8 redimerization

148 We tested if MpUVR8 interacts with MpRUP, the putative ortholog of AtRUP1 and AtRUP2
149 (Gruber et al., 2010; Clayton et al., 2018). MpUVR8 and MpRUP exhibited interaction in yeast
150 two-hybrid (Fig. 2A and B) and LCI assays (Fig. 2C, D), and MpRUP co-purified with GFP-
151 MpUVR8 in affinity-purification coupled with mass spectrometry (AP-MS) (fig. S2). We further
152 assayed if MpRUP facilitates MpUVR8 redimerization in Marchantia. In wild-type Tak-1 plants,
153 MpUVR8 dimer amount was strongly reduced upon exposure to UV-B, then reverted to initial
154 levels within approximately 1 h once under -UV-B conditions (Fig. 2E). However, in a Mp*rup*

155 mutant generated using CRISPR/Cas9 mutagenesis in the Tak-1 background (fig. S3), MpUVR8
156 dimer levels recovered slowly and did not reach "-UV" ground state levels even after 6 h (Fig. 2E).
157 We thus conclude that MpRUP facilitates MpUVR8 redimerization, indicating a conserved
158 mechanism for negative feedback regulation of UVR8 activity.
159

160 ## MpUVR8 and MpRUP antagonistically regulate UV-B-dependent growth, pigment accumulation,
161 and acclimation

162 To explore the phenotypic consequences of MpUVR8 and MpRUP action, we established robust
163 UV-B conditions for phenotypic and molecular analysis. Under continuous white light, no striking
164 differences were detectable between Tak-1, Mp*uvr8*, and Mp*rup* (Fig. 3A and fig. S4). However,
165 when exposed to white light supplemented with narrowband UV-B (1.5 µmol m^{-2} s^{-1}), Tak-1
166 exhibited a slight growth inhibition and slight accumulation of pigments (Fig. 3A and fig. S4A).
167 These responses were reduced, if not absent, in Mp*uvr8* mutant and MpRUP^{OE} overexpression
168 lines (Fig. 3A and fig. S4A, F). By sharp contrast, Mp*rup* mutants exhibited a striking UV-B-
169 hyperresponsive photomorphogenic phenotype, with extreme growth inhibition and strong
170 pigmentation of the thallus specifically under UV-B (Fig. 3A and fig. S4A) (Clayton et al., 2018),
171 similar to transgenic lines overexpressing Mp*UVR8.1* or Mp*UVR8.2* photoreceptors (fig. S4A, E).
172 We conclude that MpRUP plays a major role in MpUVR8 inactivation to sustain growth under
173 UV-B.

174 To directly assess the effect of MpUVR8-mediated acclimation on photoprotection, we
175 measured F_v/F_m representing the maximum quantum yield of photosystem II (PSII) (Murchie and
176 Lawson, 2013). Tak-1, Mp*uvr8*, and Mp*rup* plants were grown for 7 days under white light
177 supplemented with narrowband UV-B (acclimated; +/-) or not (non-acclimated; -/-) (Fig. 3B).
178 Acclimated and non-acclimated plants were then exposed to 1 h of broadband UV stress (+/+ and
179 -/+, respectively). We measured F_v/F_m before and after UV stress in both acclimated and non-
180 acclimated plants (Fig. 3B). Non-stressed Tak-1, Mp*uvr8*, and Mp*rup* displayed an F_v/F_m value
181 close to 0.8 (Fig. 3C), which is characteristic of healthy Marchantia plants (Messant et al., 2023).
182 When exposed to UV stress, F_v/F_m decreased significantly and to the same extent in non-acclimated
183 plants of all genotypes (Fig. 3C), suggesting photoinhibition resulting from PSII damage. However,
184 applying the same UV stress treatment on acclimated plants revealed a UVR8-dependent
185 photoprotective effect: in Tak-1 and even more so in Mp*rup*, F_v/F_m following UV-B stress was

186 higher in acclimated compared to non-acclimated plants, but not in Mp*uvr8* (Fig. 3C).
187 Mp*UVR8.1*^{OE} and Mp*UVR8.2*^{OE} overexpression lines were similar to Mp*rup*, whereas Mp*RUP*^{OE}
188 overexpression lines phenocopied Mp*uvr8* (fig. S4B).

189 Next, we tested the survival rates of Tak-1, Mp*uvr8*, and Mp*rup* under UV-B stress. Plants
190 were acclimated or not under narrowband UV-B for 7 days, followed by a 7- or 9-h broadband UV-
191 B stress treatment, after which all plants were returned to white light for 7 days of recovery (Fig.
192 3D). Without acclimation, Tak-1, Mp*uvr8*, and Mp*rup* did not survive subsequent UV-B stress
193 (Fig. 3E). Acclimated wild-type plants did not survive the 9-h UV-B stress treatment but some
194 gemmalings resumed growth after 7 h of UV-B stress. Mp*rup* mutants recovered more than Tak-1
195 under both stress treatments (Fig. 3E and fig. S4C, D), indicating enhanced UV-B protection. By
196 contrast, the Mp*uvr8* mutant did not survive the UV-B stress treatment even with prior UV-B
197 acclimation, demonstrating that UV-B photoprotection was dependent on MpUVR8 (Fig. 3E).
198 Complementing the Mp*uvr8-1* mutant with a *Pro*$_{\mathrm{Mp}UVR8}$*:*Mp*UVR8* construct restored UV-B stress
199 survival in acclimated plants (fig. S4C). By contrast, overexpression of MpRUP (Mp*RUP*^{OE})
200 phenocopied the Mp*uvr8* mutant phenotype (fig. S4D).

201 We prepared methanolic extracts from gemmalings and measured the absorption spectra
202 between 280–400 nm to detect UV-absorbing compounds. There was a broad peak in UV-
203 absorbance at ~340 nm for UV-B-exposed Tak-1 plants, which was absent for the Mp*uvr8* mutant
204 (Fig. 3F), indicating Marchantia plants accumulate UV-absorbing compounds in a UV-B- and
205 UVR8-dependent manner. Consistent with their enhanced UV-B acclimatory response and
206 resulting UV-B tolerance, extracts from UV-B-exposed Mp*rup* mutants had an even greater peak
207 in UV absorption (Fig. 3F). Notably, the Mp*uvr8-1* Mp*rup-2* double mutant exhibited
208 photoprotection and UV-absorbing capacity comparable to the Mp*uvr8-1* single mutant (fig. S5),
209 demonstrating that the enhanced photoprotection and UV-B-absorbing capacity of Mp*rup* is
210 dependent on MpUVR8. Next, we performed untargeted metabolomics of 9-day-old Tak-1,
211 Mp*uvr8*, and Mp*rup* grown in white light for 7 days and exposed or not to supplemental UV-B for
212 2 days, following which we detected a total of 554 metabolites (table S1). Fifty-eight metabolites
213 accumulated in response to UV-B in Tak-1 that were not observed in Mp*uvr8* (fig. S6A, table S2).
214 Over half of these (30) were assigned to compounds from the shikimate-phenylpropanoid
215 biosynthetic pathway, whereas metabolites from that pathway represented only about a quarter of
216 all compounds detected (151/609) (fig. S6B and table S2). Unlike in Arabidopsis whereby sinapate

217 esters play a major role in UV-B photoprotection (Leonardelli et al., 2024), no sinapate esters were
218 detected in Marchantia (fig. S6C, table S1). However, UV-B-absorbing flavone glycosides (e.g.
219 apigenin-7-glucoside, luteolin 7-O-glucuronide) accumulated in a MpUVR8-dependent manner
220 under UV-B, and even more so in Mp*rup* (fig. S6C-E, table S2), consistent with previous reports
221 (Clayton et al., 2018; Soriano et al., 2019). In addition to 28 of the 58 compounds that accumulated
222 in response to UVR8 activation in Tak-1, 60 compounds did so specifically in Mp*rup* likely due to
223 its hyperresponsiveness to UV-B (fig. S6A).
224

225 ## Mp*cop1* mutants exhibit constitutive photomorphogenesis and UV-B tolerance

226 Interaction of UVR8 with the COP1/SPA E3 ligase complex and its subsequent inactivation is a
227 key step in UV-B signal transduction in Arabidopsis (Favory et al., 2009; Yin et al., 2015; Lau et
228 al., 2019). MpCOP1 and MpSPA interacted in yeast two-hybrid assays, both in the absence and
229 presence of UV-B (Fig. 4A) (Zhang et al., 2021). By contrast, MpUVR8 interacted with MpCOP1
230 specifically under UV-B in yeast two-hybrid (Fig. 4A), LCI (Fig. 4B), and AP-MS assays (fig. S2).
231 Arabidopsis *cop1* null mutants have a seedling-lethal phenotype (McNellis et al., 1994) and
232 no Marchantia Mp*cop1* mutant has been recovered until now (Zhang et al., 2021). We generated
233 two viable Mp*cop1* null alleles using CRISPR/Cas9 mutagenesis (fig. S3). These mutants displayed
234 stunted growth, delayed development, and reduced gemmae production compared to Tak-1 when
235 grown under standard conditions (Fig. 5A). Whereas the Mp*cop1* mutants developed gemma cups
236 and gemmae and thus could complete their asexual life cycle, they failed to complete their sexual
237 life cycle because antheridiophores did not develop when induced under continuous white light
238 supplemented with far-red light.
239 Mp*cop1* mutants exhibited constitutively enhanced photoprotection, as evidenced by their
240 elevated F_v/F_m ratios after UV-B stress (Fig. 5B). The strong constitutively photomorphogenic
241 phenotype and enhanced photoprotection of Mp*cop1* agreed with how Mp*cop1* survived prolonged
242 broadband UV-B stress, both with or without acclimation (Fig. 5C; note that the plants are viable
243 as determined by non-stressed levels of F_v/F_m after recovery). Absorption spectra of methanolic
244 extracts also revealed constitutive hyperaccumulation of UV-absorbing compounds in Mp*cop1*
245 (Fig. 5D). Thus, MpCOP1 activity as key repressor of photomorphogenesis is evident in
246 Marchantia.
247

248 Mp*spa* mutants show only a minor constitutively photomorphogenic growth phenotype, but
249 strongly enhanced UV-B tolerance
250 To investigate the role of the single MpSPA protein, we generated two independent CRISPR/Cas9
251 knockout alleles (fig. S3). Surprisingly, both Mp*spa* alleles exhibited a phenotype comparable to
252 Tak-1 under both white light and white light supplemented with UV-B (Fig. 5A). This is in stark
253 contrast to the strong constitutively photomorphogenic phenotype observed for the Mp*cop1* mutant
254 (Fig. 5A) and Arabidopsis *spa* quadruple mutants (Ordonez-Herrera et al., 2015).
255 Furthermore, we tested the UV-B acclimation response of Mp*spa* mutants. Mp*spa* showed
256 enhanced basal UV-B tolerance when compared to wild type ("-/+", Fig. 5B), as well as after UV-
257 B acclimation ("+/+", Fig. 5B). Mp*spa* mutants also showed an increased survival rate after
258 prolonged UV-B stress if plants were previously acclimated to low UV-B (Fig. 5C). In accordance
259 with their improved UV-B stress tolerance, Mp*spa* mutants constitutively accumulated more UV-
260 absorbing compounds which became further pronounced upon UV-B-mediated acclimation (Fig.
261 5D).
262 As enhanced UV-B-acclimation of Mp*spa* resembled Mp*rup* mutants, we investigated
263 whether MpSPA function was also associated with MpUVR8 redimerization. However, in contrast
264 to Mp*rup*, Mp*spa* showed efficient MpUVR8 redimerization (fig. S7A). Additionally,
265 overexpression of Mp*SPA* and Mp*COP1* reduced basal UV-B tolerance but did not abolish UV-B-
266 induced photoprotection, in contrast to Mp*RUP* overexpression (fig. S7B-D). We conclude that
267 MpCOP1 activity as a repressor of photomorphogenesis is not fully dependent on MpSPA, and that
268 the absence of MpSPA enhances UV-B tolerance.
269
270 MpUVR8 signaling components mediate transcriptional changes in response to UV-B
271 We analyzed the UVR8-mediated transcriptome in 7-day-old Marchantia gemmalings in response
272 to 3 h of narrowband UV-B (tables S3 and S4). In Tak-1, we identified 480 and 114 genes up- and
273 downregulated by UV-B, respectively ($|\log_2$ fold-change$| > 1$; p-adj < 0.05), which all exhibited
274 MpUVR8- and MpCOP1-dependent expression changes (tables S5A, B, and S6), thus representing
275 the transcriptional MpUVR8 signaling output.
276 In Tak-1, Mp*rup*, and Mp*spa*, we identified a combined total of 756 UV-B-induced genes
277 and 298 UV-B-repressed genes ($|\log_2$ fold-change$| > 1$; p-adj < 0.05), with substantial overlaps
278 between the genotypes (Fig. 6A-C, and tables S5A, B, and S6). Interestingly, induction or

279 repression of transcripts after 3 h of UV-B was enhanced in Mp*rup* and Mp*spa* compared to Tak-
280 1 (Fig. 6C), consistent with their UV-B hyper-responsive phenotypes (Fig. 3 and Fig. 5). Consistent
281 with this, over two-thirds of genes that were up- or downregulated (│$\log_2$ fold-change│ > 1)
282 specifically in Mp*rup* and Mp*spa* ("unique Mp*rup*" and "unique Mp*spa*") were up- or
283 downregulated in Tak-1 as well when considering a lower fold-change threshold (│$\log_2$ fold-
284 change│ > 0 but <1; p-adj < 0.05) (Fig. 6A, B). Notably, whereas the transcriptomic profile of the
285 Mp*cop1-1* mutant was unresponsive to UV-B, it resembled the profile of UV-B-responsive
286 genotypes after UV-B exposure, with a large portion of genes constitutively up- or downregulated
287 (Fig. 6C, D). These data support the role of MpCOP1 as a repressor of UV-B photomorphogenesis
288 and COP1-inactivation by UVR8 as a key mechanism for UV-B-responsive gene expression
289 changes.

290 Using hierarchical clustering, we defined seven major clusters of gene expression changes
291 upon UV-B exposure (Fig. 6C, D, and table S6). Clusters 1 and 5 contain UV-B-downregulated
292 genes, with gene expression in Mp*cop1* that is constitutively down- or upregulated, respectively.
293 Cluster 7 consists of UV-B-downregulated genes that are more highly expressed in Mp*spa*. Clusters
294 4 and 6 contain genes that are induced after 3 h of UV-B in wild type, Mp*rup*, and Mp*spa*, but not
295 in Mp*uvr8* and Mp*cop1*, and their constitutive expression in Mp*cop1* is either elevated or
296 comparable in comparison to that in wild type, respectively. Clusters 2 and 3 contain genes induced
297 after 3 h of UV-B exposure in wild type, with hyper-induced expression in Mp*spa* and Mp*rup*,
298 respectively. We profiled the expression of components of the UVR8 pathway in the data: Mp*HY5*,
299 Mp*RUP*, and Mp*COP1* (cluster 2) were upregulated upon UV-B in wild type (table S6), whereas
300 Mp*UVR8* was constitutively expressed.
301

302 ## MpSPA plays a minor role in repressing visible light photomorphogenesis compared to MpCOP1

303 In Arabidopsis, *spa1234* (*spaQn*) quadruple mutants undergo constitutive photomorphogenesis
304 with a phenotype similar to strong *cop1* mutants (such as *cop1-1*) and stronger than the weak *cop1-*
305 *4* allele (Fig. 7A) (McNellis et al., 1994; Laubinger et al., 2004; Ordonez-Herrera et al., 2015).
306 However, Marchantia Mp*spa* mutants exhibited only a minor growth phenotype in white light
307 compared to the strongly affected Mp*cop1* mutants (Fig. 7A, Fig. 5A). Thus, we investigated the
308 transcriptome profile Mp*spa* and Mp*cop1* mutants in more detail.

309 By comparing white light–grown Mp*cop1* and Mp*spa* versus Tak-1, we found that in
310 Mp*cop1*, 1,256 and 1,898 genes were significantly up- or downregulated ($|\log_2$ fold-change$| > 1$;
311 p-adj < 0.05), respectively (Fig. 7B, C). By stark contrast, only 60 genes were upregulated and 15
312 genes were downregulated in Mp*spa* using the same threshold criteria (Fig. 7B, C, and table S5C,
313 D), which is significantly different from Arabidopsis, where over 7,000 differentially expressed
314 genes (DEGs) were observed between the *spaQ* mutant and the wild type (Pham et al., 2020). Of
315 those genes dysregulated in Mp*spa*, 40 out of 60 and 12 out of 15 genes were also up- and
316 downregulated, respectively, in Mp*cop1*. We further checked if genes dysregulated in Mp*cop1* but
317 not in Mp*spa* were in fact dysregulated in Mp*spa* but at a lower fold-change threshold. Indeed, out
318 of the 1,256 upregulated genes in Mp*cop1*, 486 were shared with Mp*spa* when considering a looser
319 threshold for genes upregulated in Mp*spa* ($|\log_2$ fold-change$| > 0$; p-adj < 0.05; Fig. 7B).
320 Similarly, out of the 1,898 downregulated genes in Mp*cop1*, 349 were also downregulated in
321 Mp*spa* (Fig. 7C). This indicates a larger overlap between genes dysregulated in Mp*cop1* and
322 Mp*spa* mutants in comparison to wild type, but also identifies clear differences between MpCOP1-
323 and MpSPA-dependent genes at the genome-wide level.
324 A broader examination of gene expression levels across wild type, Mp*cop1*, and Mp*spa*
325 genotypes confirmed that, although the overall profile of Mp*spa* was similar to wild-type, many
326 transcripts had levels that were intermediate between Tak-1 and Mp*cop1* (Fig. 7D and table S7).
327 Using hierarchical clustering, we defined 11 main clusters of gene expression (Fig. 7E), specifically
328 four for Mp*cop1*-upregulated genes (clusters 1, 2, 7 and 10), six for Mp*cop1*-downregulated genes
329 (clusters 3, 4, 5, 6, 8 and 9), and a small cluster of genes specifically upregulated in Mp*spa* (cluster
330 11). Interestingly, the cluster groups defined by Mp*cop1*-up- and downregulated patterns of gene
331 expression could be discriminated by the extent to which expression in Mp*spa* aligned with the
332 expression in Mp*cop1* (Fig. 7E).
333 Finally, since we observed that the regulation of many genes was dependent on MpCOP1
334 under white light, and we established that MpCOP1 has a conserved role as a repressor of
335 photomorphogenesis, we tested if genes dysregulated in Mp*cop1* were induced by UV-B in UV-
336 B-responsive genotypes. We observed that most genes upregulated under white light in Mp*cop1*
337 were induced by UV-B in Tak-1, Mp*rup*, or Mp*spa* (Fig. 7D), whereas many genes constitutively
338 downregulated in Mp*cop1* were repressed by UV-B. However, some of the Mp*cop1*-

339 downregulated genes were induced after 3 hours of UV-B, suggesting more complex dynamics
340 between induction under UV-B and steady-state levels in Mp*cop1*.
341 Overall, our analysis shows that whereas MpCOP1 plays a major role in repressing the
342 light-inducible transcriptome of Marchantia, MpSPA plays a minor yet detectable role.
343

344 ## MpHY5 promotes MpUVR8 signaling

345 The induction of Mp*HY5* expression is UV-B- and MpUVR8-dependent, repressed by both
346 MpRUP and MpSPA, and Mp*HY5* is constitutively upregulated in the Mp*cop1-1* mutant (table S6).
347 To test the role of MpHY5 in Marchantia, we generated Mp*hy5* knockout mutants by CRISPR/Cas9
348 (fig. S3). We further investigated the photoprotection and UV-B-absorbing capacity of Mp*hy5*
349 mutants. Mp*hy5* mutants showed slightly reduced basal photoprotection, as determined by
350 measuring the F_v/F_m ratio after UV-B stress exposure (-/+; Fig. 8A). Interestingly, and in contrast
351 to Arabidopsis *hy5 hyh* double mutants (Leonardelli et al., 2024), Mp*hy5* mutants were able to
352 acclimate to UV-B (+/+ versus -/+; Fig. 8A), but Mp*hy5* mutants nevertheless showed a
353 significantly reduced capacity to protect their photosynthetic machinery from subsequent UV-B-
354 induced damage compared to UV-B-acclimated wild type (+/+; Fig. 8A). In agreement, UV-B-
355 acclimated Mp*hy5* mutants were less tolerant to 7 h of UV-B stress than Tak-1 (Fig. 8B). We
356 further measured the UV-B absorbance profiles of methanolic extracts from different genotypes
357 and found that, consistent with the reduced photoprotection observed in UV-B-exposed Mp*hy5*,
358 Mp*hy5* accumulated slightly less UV-B-absorbing compounds compared to Tak-1 (Fig. 8C).
359 To further understand how MpHY5 promotes MpUVR8 signaling, we performed another
360 RNA-seq experiment with 7-day-old Tak-1 and Mp*hy5-1* Marchantia gemmalings exposed or not
361 to 3 h of narrowband UV-B (tables S3, S4, S8, and S9). Using heatmap analysis and hierarchical
362 clustering, we examined the 501 genes regulated upon UV-B exposure in Tak-1 and/or Mp*hy5-1*
363 ($|\log2 \text{ fold-change}| > 1$; p-adj < 0.05) (table S9). This analysis revealed 10 major clusters of gene
364 expression changes in response to UV-B exposure (Fig. 8D, and fig. S8). Notably, few genes were
365 entirely dependent on Mp*HY5*, though certain trends were observed where some genes showed
366 reduced or enhanced UV-B-induced expression compared to Tak-1. Mp*HY5-1* (one base deletion,
367 see fig. S3) and Mp*COP1* were hyperinduced in Mp*hy5-1* (cluster 3), while the induction of
368 Mp*RUP* was unaffected by the Mp*hy5-1* mutation (cluster 1). Most UV-B-induced genes were
369 constitutively upregulated in Mp*cop1-1* (Fig. 8D and table S5), and we noticed that the most

370 MpHY5-dependent genes (clusters 2 and 7) were associated with the highest levels of constitutive
371 upregulation in Mp*cop1*, while the genes that showed the most hyperinduction in Mp*hy5* were
372 associated with the lowest constitutive expression levels in Mp*cop1* (Fig. 8D, fig. S9, and table S8).
373 This is in agreement with an evolutionary conservation of the COP1-HY5 regulatory module in
374 Marchantia photomorphogenesis. Taken together, our data indicate that MpHY5 acts
375 antagonistically to MpCOP1 and is involved in mediating UVR8-responsive gene expression in
376 Marchantia, although to a much lesser extent than that facilitated by HY5 and HYH in Arabidopsis,
377 suggesting that other transcription factors play major roles in UVR8 signaling in Marchantia.
378

379 ## DISCUSSION

380 UV-B exposure elicits UVR8-dependent transcriptional changes underlying UV-B acclimation
381 phenotypes in plants (Kliebenstein et al., 2002; Brown et al., 2005; Favory et al., 2009; Tilbrook
382 et al., 2016; Tavridou et al., 2020a; Hu et al., 2024; Dannay et al., 2025). The present study defines
383 the MpUVR8-mediated genome-wide transcriptional response and provides physiological
384 evidence for how MpUVR8 regulates acclimation and UV-stress tolerance in Marchantia using a
385 broad panel of knock-out mutants in the UVR8 signaling pathway. Importantly, our study further
386 demonstrates that although core components of UV-B signaling are conserved, their regulatory
387 interactions and functions have significantly diversified.

388 In contrast to that in Arabidopsis and the moss *Physcomitrium patens* (hereafter
389 Physcomitrium), MpUVR8 has been reported to form weaker dimers and increased levels of
390 monomer *in vivo* in the absence of UV-B, which is observed when analyzing MpUVR8
391 dimer/monomer ratio by SDS-PAGE and immunoblotting using samples that are not heat-
392 denatured before electrophoresis (Soriano et al., 2018). Although this type of assay is accurate for
393 the dimer/monomer status of wild-type AtUVR8 (Rizzini et al., 2011; Heijde and Ulm, 2013;
394 Heilmann and Jenkins, 2013; Findlay and Jenkins, 2016; Moriconi et al., 2018), it can make weak
395 dimeric UVR8 mutant variants appear monomeric, whereas *in vitro* assays (Christie et al., 2012;
396 Wu et al., 2012; Heijde et al., 2013) as well as more stringent assays using protein-protein
397 crosslinking identify these variants as homodimeric *in vivo* (Rizzini et al., 2011; Podolec et al.,
398 2021b). Thus, we employed crosslinking to show that MpUVR8 is indeed dimeric *in vivo* in the
399 absence of UV-B, consistent with the UV-B-dependent dimer-to-monomer transition being a
400 conserved feature of the UVR8 photocycle (Rizzini et al., 2011; Tilbrook et al., 2016; Podolec et

401 al., 2021a). Furthermore, we provide evidence that negative feedback regulation through MpRUP-
402 facilitated redimerization of MpUVR8 is conserved in Marchantia. Consistent with this, the Mp*rup*
403 mutant displayed a strong UV-B photomorphogenic phenotype, characterized by growth inhibition
404 resulting in a small size, a strong pigmentation of the thallus, and higher UV-B stress tolerance
405 associated with increased accumulation of UV-absorbing compounds (see also Clayton et al., 2018).
406 Interestingly, this conditional phenotype of Mp*rup* specifically under UV-B phenocopies the
407 constitutive Mp*cop1* phenotype, in agreement with active UVR8-mediated inactivation of COP1
408 underlying UV-B signaling (Yin et al., 2015; Lau et al., 2019). We further show that GFP-
409 MpUVR8 expressed under its own promoter localizes mainly to the cytosol and displays UV-B-
410 dependent nuclear accumulation in Marchantia, confirming findings using a *Citrine*-Mp*UVR8*
411 overexpression line (Kondou et al., 2019). Thus, we conclude that the homodimeric ground state
412 of UVR8, its UV-B dependent monomerization, nuclear accumulation, and COP1 inactivation, as
413 well as negative feedback regulation of UVR8 through RUP-facilitated redimerization are well-
414 conserved in Marchantia.

415 In flowering plants, COP1 forms an E3 ligase complex together with SPA proteins, which
416 together function as suppressors of photomorphogenesis; i.e. COP1 requires SPA proteins to
417 function (Hoecker, 2017; Podolec and Ulm, 2018). Since non-plant COP1 orthologs are not
418 regulated by light, it is hypothesized that the evolution of SPA proteins was a crucial step in
419 enabling photoreceptor-mediated regulation of COP1/SPA complex activity (Ranjan et al., 2014;
420 Balcerowicz et al., 2017; Podolec and Ulm, 2018). Active phytochrome and cryptochrome
421 photoreceptors directly interact with SPA proteins, which represses the E3 ligase activity of the
422 COP1/SPA complex (Hoecker, 2017; Podolec and Ulm, 2018). In agreement, Arabidopsis
423 quadruple *spa* mutants exhibit strong constitutive photomorphogenesis (Ordonez-Herrera et al.,
424 2015). However, it is of note that *spa* quadruple null mutants can complete their life cycle whereas
425 *cop1* null mutants cannot (McNellis et al., 1994; Ordonez-Herrera et al., 2015), suggesting that
426 COP1 can function partially in a SPA-independent manner. COP1, but not SPA proteins, are also
427 necessary for transient gene expression changes upon exposure to UV-B (Favory et al., 2009).
428 Recently, the role of COP1/SPA has started to be explored in more phylogenetically distant land
429 plant lineages such as bryophytes, including Physcomitrium (Kreiss et al., 2023). A Physcomitrium
430 Pp*cop1_9x* mutant lacking all nine PpCOP1(a-i) orthologs was viable and displayed a rather minor
431 growth phenotype, certainly much less severe than the Arabidopsis *cop1* mutant phenotypes

432 (Kreiss et al., 2023). In this study, we analyzed mutants of the single Mp*COP1* gene in light-grown
433 Marchantia plants and found that, although they completed their asexual life cycle, they exhibited
434 profound transcriptome changes and a severe constitutively photomorphogenic phenotype.
435 Additionally, consistent with the described role of COP1 in UV-B signaling in Arabidopsis and
436 Chlamydomonas (Oravecz et al., 2006; Favory et al., 2009; Allorent et al., 2016; Tilbrook et al.,
437 2016), transient gene expression changes upon exposure to UV-B were dependent on MpCOP1.
438 The Marchantia genome contains a single gene encoding MpSPA that interacts with MpCOP1 and
439 MpCRY (Zhang et al., 2021). Surprisingly, Mp*spa* null mutants exhibited at most a mild
440 constitutively photomorphogenic phenotype in white light, unlike Mp*cop1*. Interestingly, in
441 Physcomitrium, a Pp*spa_ab* double mutant displayed an intermediate phenotype between that of
442 the wild type and Pp*cop1_9x*. This suggests that SPA proteins indeed play a lesser role in repressing
443 light signaling in bryophytes compared to in angiosperms (Huang et al., 2013; Ordonez-Herrera et
444 al., 2015; Artz et al., 2019; Kreiss et al., 2023) and that high dependence of COP1 on the accessory
445 SPA proteins evolved later, meaning that SPA protein evolution is separate to the evolution of
446 COP1 activity regulation by light. This is further supported by the discovery of the UVR8- and
447 cryptochrome photoreceptor–mediated COP1 inactivation mechanism of high-affinity competitive
448 binding and displacement of COP1 substrates (Lau et al., 2019; Ponnu et al., 2019; Trimborn et al.,
449 2025). Moreover, complementation of corresponding Arabidopsis mutant phenotypes was possible
450 with a Physcomitrium COP1 ortholog but not a SPA ortholog (Ranjan et al., 2014), further
451 indicating the divergence of SPA function between evolutionary lineages.

452 Enhanced UV-B-induced changes in gene expression, increased accumulation of UV-
453 absorbing compounds, and enhanced UV-B acclimation and photoprotection against UV stress in
454 Mp*spa* mutants compared to that in wild type revealed a repressor role for SPA in the UV-B
455 signaling pathway of Marchantia. This is similar to Mp*rup* mutants, although long-term growth
456 under UV-B was not as strongly inhibited in Mp*spa*. MpSPA also did not facilitate MpUVR8
457 redimerization like observed for MpRUP. Several hypotheses can be proposed to explain the
458 Mp*spa* phenotype. It has been reported that MpSPA can promote the ubiquitination of MpHY5 by
459 MpCOP1 (Zhang et al., 2021). Consequently, the lack of MpSPA could result in reduced
460 ubiquitination of MpHY5 by MpCOP1, leading to higher activation of downstream genes. Also,
461 UV-B-activated MpUVR8 may inactivate MpCOP1 more strongly in the absence of MpSPA,
462 leading to an enhanced UV-B response. MpSPA might function by "shielding" the MpCOP1/SPA

463 complex from being inhibited by MpUVR8 under UV-B by providing an additional UVR8-
464 irrepressible activity. Moreover, it has been suggested that SPA proteins promote the
465 phosphorylation of several proteins involved in light signaling in Arabidopsis, including UVR8
466 and HY5 (Wang et al., 2021; Liu et al., 2024). Therefore, in the event such activity is conserved,
467 the absence of MpSPA may affect the phosphorylation status and activity of light signaling
468 components, enabling the Mp*spa* mutant to respond more strongly to UV-B and to produce more
469 "sunscreen" metabolites. Future work is required to elucidate the precise mechanism by which
470 MpSPA exerts its repressive effect on UV-B signaling in Marchantia, and to determine if a similar
471 SPA protein function exists in Arabidopsis or whether this represents a species-specific UV-B
472 response regulatory mechanism. Overall, genetic analysis of COP1/SPA function suggests that,
473 whereas the role of COP1 is widely conserved within the green lineage, the importance of SPA
474 proteins in regulating COP1 activity and repressing photomorphogenesis increased during plant
475 evolution.

476 It is of note that the role and importance of the transcriptional regulators HY5/HYH in
477 UVR8-signaling has also changed during plant evolution. HY5 is a major player in UVR8-
478 signaling in Arabidopsis (Ulm et al., 2004; Brown et al., 2005; Oravecz et al., 2006; Binkert et al.,
479 2014), whereas the closest Chlamydomonas homolog of HY5, CrBLZ3, plays only a minor role in
480 the algal UV-B response (Dannay et al., 2025). Instead, the B-box family transcription factor and
481 CrCOP1 substrate CrCONSTANS is the main player in the CrUVR8 signaling pathway (Gabilly
482 et al., 2019; Tokutsu et al., 2019; Dannay et al., 2025). In Marchantia, MpHY5 controls a subset
483 of MpUVR8-induced genes but has a less prominent role than its counterpart in Arabidopsis. Other
484 transcription factor(s) mediating MpUVR8 signaling remain to be identified.

485 In conclusion, our study provides a comprehensive understanding of the UV-B perception
486 and signaling mechanisms in the liverwort model organism Marchantia. Our findings further
487 confirm and strengthen the notion that the UVR8 photoreceptor and its associated signaling
488 components are conserved in Marchantia, highlighting the evolutionary importance of this pathway
489 in mediating UV-B responses across land plants. Our analysis of the COP1/SPA E3 ligase complex
490 and its HY5 substrate in Marchantia also revealed divergences in the functions of this
491 photomorphogenesis-repressing complex.
492

493 MATERIALS AND METHODS

494 **Plant materials**

495 The *Marchantia polymorpha* accessions Takaragaike-1 (Tak-1) and Tak-2 were used as male and
496 female wild type, respectively (Ishizaki et al., 2008). The Mp*uvr8-1* mutant was described
497 previously (Kondou et al., 2019), whereas the following mutants were generated using CRISPR–
498 Cas9-mediated mutagenesis (Sugano et al., 2018; Sauret-Güeto et al., 2020): Mp*rup-2,* Mp*rup-3,*
499 Mp*cop1-1,* Mp*cop1-2,* Mp*spa-9,* Mp*spa-10,* Mp*hy5-1,* Mp*hy5-3,* and Mp*hy5-7*. Two different
500 gene-specific guide RNAs (gRNAs, see table S10) were selected using the CRISPRdirect
501 (https://crispr.dbcls.jp/) or CasFinder (https://marchantia.info/tools/casfinder/) tools (Aach et al.,
502 2014). Corresponding complementary DNA oligos were annealed and ligated into the BsaI sites of
503 pMpGE_En03, then subcloned to the binary vector pMpGE010 (Sugano et al., 2018) using
504 Gateway LR Clonase II (Thermo Fisher Scientific). To generate the Mp*hy5* mutants,
505 complementary oligos were inserted into BbsI sites of the L1_lacZgRNA-Ck2 and L1_lacZgRNA-
506 Ck3 vectors, respectively, after which these were recombined by SapI restriction enzymes with the
507 L1_HyR-Ck1 and L1_Cas9-Ck4 vector into the pCsA acceptor plasmid using Golden Gate Loop
508 Assembly (Sauret-Güeto et al., 2020). Following transformation, frame-shift and early stop codon
509 mutants were identified using PCR genotyping and Sanger sequencing (table S10 and fig. S3).

510 To generate *Pro*$_{\text{Mp}UVR8}$:*GFP*-Mp*UVR8* reporter lines, we modified the previously described
511 pMpGWB301-MpUVR8 genomic construct (Kondou et al., 2019). The vector was digested with
512 MluI and HpaI and the GFP coding sequence was ligated immediately upstream of the Mp*UVR8*
513 start codon. To create Pro$_{\text{Mp}CHS2}$:*LUC* reporter lines, the predicted Mp*CHS2* promoter including
514 5′UTR sequence (3,000 bp region upstream of the Mp*CHS2* start codon) was amplified from Tak-
515 1 genomic DNA and the PCR product was inserted into pDONR207 via Gateway BP reaction. The
516 *Pro*$_{\text{Mp}CHS2}$ sequence was then transferred into the pMpGWB331 vector by LR reaction, followed
517 by transformation into the Tak-1 wild-type background. To create *Pro*$_{\text{Mp}CHS2}$*:LUC* lines in the
518 Mp*uvr8-1* and Mp*rup-1* backgrounds, Tak-1/*Pro*$_{\text{Mp}CHS2}$*:LUC* was first crossed with Tak-2 to obtain
519 Tak-2/*Pro*$_{\text{Mp}CHS2}$*:LUC* in female background, and then the male Mp*uvr8-1* or Mp*rup-2* mutants
520 were crossed with the female Tak-2/*Pro*$_{\text{Mp}CHS2}$*:LUC* line. To generate overexpression lines in Tak-
521 1, the coding sequences including stop codons of Mp*UVR8.1*, Mp*UVR8.2*, Mp*RUP*, Mp*COP1*, and
522 Mp*SPA* were first cloned into the pDONR207 entry vector via BP reaction, then transferred via LR
523 reaction into the pMpGWB336 destination vector containing the *ELONGATION FACTOR 1α*

524 (Mp*EF1α*, Mp3g23400) promoter and an N-terminal Red Fluorescent Protein (RFP) tag.
525 Agrobacterium-mediated Marchantia thallus transformation was performed as previously
526 described (Kubota et al., 2013). Marchantia spore transformation was used to generate Mp*hy5*
527 mutants as previously described (Chiyoda et al., 2008).
528 Mp*uvr8-1* Mp*rup-2* Cas9-free double mutants were generated by crossing Mp*rup-2* (male)
529 with Tak-2 to select for female lines, followed by crossing Mp*uvr8-1* (male) with Mp*rup-2*
530 (female), as previously described (Mulvey and Dolan, 2023). For those plants where the inheritance
531 of the parental alleles was confirmed, replica plating on plates with and without hygromycin was
532 repeated to further verify the absence of the Cas9 transgene.
533

534 **Growth conditions and light treatments**

535 For maintenance, Marchantia plants were cultured aseptically on half-strength Gamborg's B5
536 medium with 1.2% (w/v) agar at 22°C under continuous white light (50 µmol m^{-2} s^{-1}) in a CLF
537 GroBank growth chamber. For UV-B acclimation experiments, continuous white light was
538 supplemented with narrowband UV-B tubes (Philips TL20W/01RS, 1.5 µmol m^{-2} s^{-1}). For UV-B
539 stress treatments, plates were irradiated under broadband UV-B tubes (Philips TL20W/12RS; 25
540 µmol m^{-2} s^{-1}).
541

542 **Crosslinking and immunoblotting**

543 Crosslinking of proteins and immunoblot analysis of 7-day-old Marchantia gemmalings was
544 performed following a modified version of a previously described method (Rizzini et al., 2011),
545 except that the extraction buffer did not contain leupeptine, dichloroisocumarin, MG115, and PSI.
546 Polyclonal rabbit anti-MpUVR8$^{(3-17)}$ antibodies raised and purified against a synthetic peptide
547 (amino acids C + 3–17: CDSKMSSNERPRRRVL) were used as the primary antibodies
548 (Eurogentec), with horseradish peroxidase (HRP)-conjugated anti-rabbit immunoglobulins (Dako
549 A/S) as secondary antibodies. The signal was revealed using ECL Select Western Blotting
550 Detection Reagent (GE Healthcare) and analyzed using an Amersham Imager 680 camera system
551 (GE Healthcare).
552

553 ## Quantitative reverse transcription PCR (RT-qPCR) analysis

554 RNA was isolated with the RNeasy Plant Mini kit (Qiagen) according to the manufacturer's
555 instructions and was treated on-column with the RQ1 RNase-Free DNase (Promega), before
556 serving as template for cDNA synthesis using the TaqMan Reverse Transcription Reagents kit
557 (Thermo Fisher Scientific) with a 1:1 mix of oligo-dT and random hexamer primers. RT-qPCR
558 was performed using the PowerUp SYBR Green Master Mix (Thermo Fisher Scientific) on a
559 QuantStudio™ 5 Real-Time PCR System (Thermo Fisher Scientific). Mp*EF1α* was used as
560 reference gene for normalization (Saint-Marcoux et al., 2015), and expression values were
561 calculated using the $2^{(-\Delta\Delta Ct)}$ method (Livak and Schmittgen, 2001). Gene-specific primers are listed
562 in table S10. Every experiment was performed using three biological replicates, and all expression
563 values were normalized against the average of untreated wild type, which was set to 1.

564

565 ## Yeast two-hybrid

566 Yeast two-hybrid assays were performed as described previously (Rizzini et al., 2011). Gateway-
567 based cloning was used to insert the Mp*UVR8.1*, Mp*UVR8.2*, Mp*RUP*, Mp*COP1*, and Mp*SPA*
568 coding sequences downstream of the LexA DNA binding domain (BD) in pBTM116-D9 (Stelzl et
569 al., 2005) or GAL4 activation domain (AD) in pGADT7-GW (Marrocco et al., 2006). The empty
570 vectors were used as negative controls. All the constructs were transformed into the yeast strain
571 L40 using the lithium-acetate protocol (Gietz et al., 2014). For the interaction assays, serial
572 dilutions of transformed yeast colonies were grown under narrowband UV-B (1.5 µmol m^{-2} s^{-1}) at
573 30°C for three days either under a WG305 (+UV-B) or a WG368 (-UV-B control) cut-off filter
574 (Schott Glaswerke). For quantification, transformed yeast colonies were grown under +UV-B or -
575 UV-B control conditions for 16 h. Ten colonies were then combined and resuspended in YPD
576 media, OD_{600} was measured, and cells were spun down and washed. The quantitative interaction
577 assay was carried out with chlorophenol red-β-D-galactopyranoside (CPRG; Roche Applied
578 Science) as substrate, according to the Yeast Protocols Handbook (Clontech, Version PR973283).

579

580 ## Affinity purification – mass spectrometry (AP–MS)

581 AP–MS was performed using a Marchantia transgenic line expressing *Pro*$_{\text{Mp}UVR8}$*:GFP*-Mp*UVR8*,
582 with wild-type Tak-1 and a *Pro*$_{\text{Mp}UBQ2}$*:mVenus* line as negative controls. Plants were grown for 7
583 days under continuous white light (50 µmol m^{-2} s^{-1}) without UV-B, or under continuous white light

584 (50 µmol m^{-2} s^{-1}) supplemented with narrowband UV-B (1.5 µmol m^{-2} s^{-1}) followed by a 20 min
585 broadband UV-B exposure (25 µmol m^{-2} s^{-1}) immediately prior to harvest. Total protein was
586 extracted and GFP-Trap agarose beads (Chromotek) were used for affinity purifications. Eluted
587 proteins were subjected to LC-MS/MS analysis.

588 Sample preparation and LC-MS/MS data acquisition: enriched proteins were submitted to
589 an on-bead digestion using trypsin. In brief, dry beads were re-dissolved in 25 µL digestion buffer
590 1 (50 mM Tris, pH 7.5, 2M urea, 1mM DTT, 5 ng/µL trypsin) and incubated for 30 min at 30 °C
591 in a Thermomixer with 400 rpm. Next, beads were pelleted and the supernatant was transferred to
592 a fresh tube. Digestion buffer 2 (50 mM Tris, pH 7.5, 2M urea, 5 mM CAA) was added to the
593 beads, after mixing the beads were pelleted, the supernatant was collected and combined with the
594 previous one. The combined supernatants were then incubated o/n at 32°C in a Thermomixer with
595 400 rpm; samples were protected from light during incubation. The digestion was stopped by
596 adding 1 µL TFA and desalted with C18 Empore disk membranes according to the StageTip
597 protocol (Rappsilber et al., 2003).

598 Dried peptides were re-dissolved in 2% ACN, 0.1% TFA (10 µL) for analysis. Samples
599 were analyzed using an EASY-nLC 1200 (Thermo Fisher) coupled to a Q Exactive Plus mass
600 spectrometer (Thermo Fisher). Peptides were separated on 16 cm frit-less silica emitters (New
601 Objective, 75 µm inner diameter), packed in-house with reversed-phase ReproSil-Pur C18 AQ 1.9
602 µm resin (Dr. Maisch). Peptides were loaded on the column and eluted for 115 min using a
603 segmented linear gradient of 5% to 95% solvent B (0 min : 5%B; 0-5 min -> 5%B; 5-65 min ->
604 20%B; 65-90 min ->35%B; 90-100 min -> 55%; 100-105 min ->95%, 105-115 min ->95%)
605 (solvent A 0% ACN, 0.1% FA; solvent B 80% ACN, 0.1%FA) at a flow rate of 300 nL/min. Mass
606 spectra were acquired in data-dependent acquisition mode with a TOP15 method. MS spectra were
607 acquired in the Orbitrap analyzer with a mass range of 300–1750 m/z at a resolution of 70,000
608 FWHM and a target value of 3×10^6 ions. Precursors were selected with an isolation window of 1.3
609 m/z (Q Exactive Plus). HCD fragmentation was performed at a normalized collision energy of 25.
610 MS/MS spectra were acquired with a target value of 10^5 ions at a resolution of 17,500 FWHM, a
611 maximum injection time (max.) of 55 ms and a fixed first mass of m/z 100. Peptides with a charge
612 of +1, greater than 6, or with unassigned charge state were excluded from fragmentation for MS^2,
613 dynamic exclusion for 30s prevented repeated selection of precursors.

614 Data analysis: raw data were processed using MaxQuant software (version 1.6.3.4,
615 http://www.maxquant.org/) (Cox and Mann, 2008) with label-free quantification (LFQ) and iBAQ
616 enabled (Tyanova et al., 2016).
617 MS/MS spectra were searched by the Andromeda search engine against a combined
618 database containing the sequences from *M. polymorpha* (MpTak_v6.1r2.protein.fasta;
619 https://marchantia.info/download/MpTak_v6.1r2/) and sequences of 248 common contaminant
620 proteins and decoy sequences. Trypsin specificity was required and a maximum of two missed
621 cleavages allowed. Minimal peptide length was set to seven amino acids. Carbamidomethylation
622 of cysteine residues was set as fixed, oxidation of methionine and protein N-terminal acetylation
623 as variable modifications. The match between runs option was enabled. Peptide-spectrum-matches
624 and proteins were retained if they were below a false discovery rate of 1% in both cases. The MS
625 data have been deposited in the ProteomeXchange Consortium via the PRIDE partner repository
626 with the dataset identifier PXD065691.
627 Statistical analysis of the MaxLFQ values was carried out using Perseus (version 1.5.8.5,
628 http://www.maxquant.org/). Quantified proteins were filtered for reverse hits and hits "identified
629 by site" and MaxLFQ values were log2 transformed. After grouping samples by condition only
630 those proteins were retained for the subsequent analysis that had three valid values in one of the
631 conditions. Missing values were imputed from a normal distribution (1.8 downshift, separately for
632 each column). Significantly enriched proteins were identified using a p-value cutoff of < 0.01 and
633 a log10 fold change threshold of ± 1.0 (table S11).
634
635 **F_v/F_m measurements**
636 Plates containing 15 gemmalings per genotype were incubated in darkness for at least 5 min, which
637 was sufficient to ensure a steady state under the plant growth conditions. A PSI (Photon Systems
638 Instruments) FluorCam 800 MF was used to measure maximum fluorescence in the dark (F_m) using
639 saturating pulses of 2000 µmol m^{-2} s^{-1} white light (400–720 nm) for 960 ms, followed by detection
640 pulses of orange-red light (620 nm) lasting 10 µs. The F_v/F_m ratio was calculated using the formula
641 $F_v/F_m = (F_m - F_o) / F_m$, where Fm represents the maximal fluorescence, and F_o represents the
642 minimal fluorescence in the dark-adapted state.
643
644 **Luciferase complementation imaging (LCI) and reporter assays**

645 LCI assays were performed as previously described (Zhou et al., 2018). Site-directed mutagenesis
646 was performed as described previously (Sawano and Miyawaki, 2000) to generate
647 MpUVR8.1^{D95N,D106N} and MpUVR8.2^{D95N,D106N}. The pCambia1300–nLUC vector was first
648 digested with BamHI and SalI, while the pCambia1300–cLUC vector was digested with KpnI and
649 SalI. Subsequently, the cDNA fragments of Mp*UVR8.1*, Mp*UVR8.2*, Mp*UVR8.1*^{D95N,D106N},
650 Mp*UVR8.2*^{D95N,D106N}, Mp*RUP*, and Mp*COP1* were cloned into the two digested vectors using
651 Gibson assembly. *Agrobacterium tumefaciens* strain GV3101 harboring the indicated
652 combinations of constructs expressing nLUC and cLUC fusion proteins were mixed in a 1:1 ratio
653 and infiltrated into *N. benthamiana* leaves. The plants were kept in the growth chamber for 2 days
654 before being incubated with 1 mM luciferin (D-luciferin sodium salt, Yeasen Biotechnology) for
655 10 min (in darkness). Luciferase activity was detected using a NightSHADE LB985 In Vivo Plant
656 Imaging System (Berthold).
657 For *Pro*$_{MpCHS2}$*:LUC* luciferase reporter assays, gemmae were transferred into 96-well plates
658 containing ½-strength Gamborg's B5 medium with 1.2% (w/v) agar and grown under at 22°C
659 continuous white light (50 µmol m^{-2} s^{-1}) in a CLF GroBank growth chamber for two days. Four-
660 µL of 1 mM luciferin were added to each well and the following day plants were exposed to UV-
661 B for 20 min and luminescence was recorded using a Centro XS LB 960 luminometer.
662

663 **Extraction of phenolic compounds, measurements of absorption spectra, and high-**
664 **performance thin-layer chromatography (HPTLC)**

665 Phenolic compounds were extracted in 100 µL of 80% (v/v) methanol from 50 mg of fresh plant
666 material homogenized using a Silamat S6 (Ivodar Vivadent). Extracts were incubated for 10 min
667 at 70°C on a shaker and centrifuged for 10 min at 12,000 *g* at room temperature (RT). A 40-µL
668 aliquot of clear supernatant from each extract was transferred to a transparent 96-well plate and
669 absorption spectra (200–1000 nm wavelengths) were measured using a TECAN Spark 10M
670 Multimode Microplate Reader. In case absorbance values exceeded the linear range, aliquots were
671 uniformly diluted with extraction buffer.
672 HPTLC was used to analyze the phenolic compound profile using silica-60 HPTLC glass
673 plates (Sigma-Aldrich), as described previously (Stracke et al., 2010; Leonardelli et al., 2024).
674

675 ## Microscopy

676 *Pro*$_{MpUVR8}$*:GFP*-Mp*UVR8* transgenic gemmalings were grown for 7 days under
677 50 µmol $m^{-2}s^{-1}$ white light and irradiated for 20 min with 25 µmol m^{-2} s^{-1} broadband UV-B.
678 Imaging was performed using a Leica Thunder Widefield microscope in both GFP and bright-field
679 modes. Z-stack images were acquired at 2-µm intervals. Image processing and Z-projection were
680 conducted using ImageJ software.

681

682 ## Transcriptome analysis

683 Gemmalings were grown for 7 days in 50 µmol m^{-2} s^{-1} white light and exposed or not to
684 supplemental UV-B (1.5 µmol m^{-2} s^{-1}) for 3 h. Total RNA was extracted using the RNeasy Plant
685 Mini kit (Qiagen) and Illumina Tru-Seq libraries were generated from cDNA and sequenced using
686 Illumina NovaSeq 100-bp single-end (table S3). Raw reads were trimmed for quality using Trim
687 Galore (v0.6.7; github.com/FelixKrueger/TrimGalore) with "-q 25 --stringency 5" as parameters.
688 Trimmed reads were mapped to the MpTak.v7.1 genome reference using STAR (v2.7.4; (Dobin et
689 al., 2013), followed by read quantification using featureCounts (Subread v2.0.1; (Liao et al., 2019).
690 The raw counts were normalized and differential expression analysis was performed using DESeq2
691 (Love et al., 2014). Genes with a $\log_2$ fold change greater than 1 and a p-adj value of less than 0.05
692 were considered as significantly differentially expressed. Genes with lower log2 fold change values
693 and p-adj < 0.05 were considered when comparing different genotypes in which gene expression
694 changes may occur at varying magnitude (table S4). Euler plots were generated using the eulerr
695 package in R. Heatmaps were generated using the heatmap.2 function in the gplots package in R.
696 The raw RNA-sequencing data has been deposited in the NCBI Gene Expression Omnibus
697 (www.ncbi.nlm.nih.gov/geo) and is accessible through GEO Series accession number GSE296364.

698

699 ## Untargeted metabolomics

700 7-day-old Marchantia gemmalings were ground in liquid nitrogen using a mortar and pestle. 50 mg
701 of tissue powder were transferred into a 1.5-mL tube and compounds were extracted with 5
702 volumes of 80% (v/v) methanol containing 0.1% (v/v) formic acid. After centrifugation, the
703 supernatant was transferred to an HPLC glass vial fitted with a conical insert. A 0.75-µL injection
704 of the extract was performed into ultrahigh performance liquid chromatography coupled to high-
705 resolution mass spectrometry (UHPLC-HRMS) equipped with an electrospray ionization (ESI)

706 source operating in negative (ESI-) ionization mode. Specifically, the system used was an Acquity
707 UPLC I-Class (Waters) interfaced with a Synapt XS QTOF (Waters). The parameters used for
708 untargeted metabolomics were based on (Defossez et al., 2023) with minor adjustments. Briefly,
709 chromatography was done on a Waters Acquity UPLC™ HSS T3 column (100 × 2.1 mm, 1.8 µm)
710 with mobile phases consisting of H2O + 0.05% (v/v) formic acid (solvent A) and acetonitrile + 0.05%
711 (v/v) formic acid (solvent B). A linear gradient from 0 to 100% B in 10.0 min at a flow rate of 0.5
712 mL/min was applied. MS detection was performed in negative electrospray ionisation using data-
713 dependent acquisition (DDA). The mass range for both MS and MS/MS was 50–1200 Da. Scan
714 times for MS and MS/MS were 0.1 and 0.05 s, respectively. The top 7 precursor ions were selected
715 for MS/MS with an intensity threshold of 15,000 counts per second. An exclusion list of the 150
716 most intense background ions was generated from a blank sample run just before the plant samples,
717 and a dynamic exclusion of 1.5 s was applied after each MS/MS acquisition. For MS/MS
718 acquisition, a ramped collision energy of 5–40 V (at *m/z* 50) and 20–70 V (at *m/z* 1200) was set.
719 The entire system and method were controlled by MassLynx 4.2 (Waters). Raw profile data were
720 first centroided in MassLynx and further converted to MzML using MSConvert (ProteoWizard).
721 We used MZmine 4.5 for feature detection, deconvolution, and alignment of DDA (data-dependent
722 acquisition) data, with noise thresholds set to 2000 for MS1 and 50 for MS2 (Schmid et al., 2023).
723 The resulting peak table and MS/MS spectral data were exported and annotated using SIRIUS 6.2
724 (Duhrkop et al., 2019), including CSI:FingerID for structural identification and CANOPUS for the
725 prediction of compound classes, superclasses, and biosynthetic pathways. Taxonomically informed
726 reannotation of molecular features was performed using the Tima R package (Rutz and Allard,
727 2025).
728

729 **Statistical analyses**

730 Statistical analyses were performed using GraphPad Software Prism 10 software (San Diego,
731 California). Statistical significance of the differences between means was determined using one-
732 or two-way analysis of variance (ANOVAs) followed by Tukey's post hoc honestly significant
733 difference (HSD) test for multiple comparisons. For metabolomics, adjusted p-values were
734 calculated and corrected using the Benjamini-Hochberg in R.
735

736 **Accession numbers**

737 Sequence data from this article can be found in the GenBank/EMBL data libraries under accession
738 numbers: Mp2g11590 (Mp*UVR8*), Mp2g18040 (Mp*RUP*), Mp5g12010 (Mp*COP1*), Mp3g25460
739 (Mp*SPA*), Mp1g16800 (Mp*HY5*), Mp2g07060 (Mp*CHS2*), Mp1g10150 (Mp*PAL1*), Mp6g00020
740 (Mp*C4H1*), Mp8g05070 (Mp*C4H2*), Mp8g05080 (Mp*C4H3*), Mp1g27780 (Mp*4CL1*),
741 Mp1g05060 (Mp*4CL2*), Mp2g22700 (Mp*CHS6*), Mp5g01410 (Mp*CHIL2*), Mp6g05290 (Mp*CHI*),
742 Mp1g26540 (Mp*F3H*), Mp3g23400 (Mp*EF1α*).

743

744 **Supplementary materials**

745 Figs. S1 to S10.

746 Tables S1 to S11.

747

748 ACKNOWLEDGEMENTS

749 We would like to thank Youichi Kondou (Kanto Gakuin University College of Science and
750 Engineering, Yokohama, Japan) for kindly providing the Mp*uvr8-1* mutant and the pMpGWB301-
751 MpUVR8 construct, Félix Rico-Reséndiz (University of Geneva) for sharing protocols and tips
752 regarding Marchantia cultivation and transformation, Yanfei Zhou (The New Zealand Institute for
753 Plant and Food Research Limited, Palmerston North, New Zealand) for precious suggestions, and
754 Anne Harzen (Max-Planck Institute for Plant Breeding Research) for MS sample preparation. The
755 RNA-seq experiments were performed at the iGE3 Genomics Platform of the University of Geneva.

756

757 FUNDING

758 This work was supported by a European Research Council Advanced Grant (DENOVO-P, project
759 no. 787613) to L.D. and a Swiss National Science Foundation grant (310030_207716) to R.U.

760

761 AUTHOR CONTRIBUTIONS

762 Y.L., R.P., and R.U. conceived and designed the research; Y.L., R.P., and R.C. performed the
763 experiments; G.G. and E.Def. performed and contributed metabolomic data; S.C.S and H.N.
764 performed and analyzed LC-MS/MS data; J.R. and L.D. contributed Mp*hy5* mutants; Y.L., R.P.,
765 E.Dem., and R.U. analyzed the data and wrote the manuscript. All authors reviewed and approved
766 the submitted manuscript.

767

768 **Competing interests**

769 The authors declare that they have no competing interests.

770

771 REFERENCES

772 **Aach J, Mali P, Church GM** (2014) CasFinder: Flexible algorithm for identifying specific Cas9 targets in
773 genomes. bioRxiv**:** 005074

774 **Allorent G, Lefebvre-Legendre L, Chappuis R, Kuntz M, Truong TB, Niyogi KK, Ulm R, Goldschmidt-**
775 **Clermont M** (2016) UV-B photoreceptor-mediated protection of the photosynthetic machinery in
776 *Chlamydomonas reinhardtii*. Proc Natl Acad Sci USA **113:** 14864-14869

777 **Artz O, Dickopf S, Ranjan A, Kreiss M, Abraham ET, Boll V, Rensing SA, Hoecker U** (2019) Characterization
778 of *spa* mutants in the moss Physcomitrella provides evidence for functional divergence of SPA
779 genes during the evolution of land plants. New Phytol **224:** 1613-1626

780 **Balcerowicz M, Kerner K, Schenkel C, Hoecker U** (2017) SPA proteins affect the subcellular localization of
781 COP1 in the COP1/SPA ubiquitin ligase complex during photomorphogenesis. Plant Physiol **174:**
782 1314-1321

783 **Binkert M, Kozma-Bognar L, Terecskei K, De Veylder L, Nagy F, Ulm R** (2014) UV-B-responsive association
784 of the Arabidopsis bZIP transcription factor ELONGATED HYPOCOTYL5 with target genes, including
785 its own promoter. Plant Cell **26:** 4200-4213

786 **Bowman JL, Kohchi T, Yamato KT, Jenkins J, Shu S, Ishizaki K, Yamaoka S, Nishihama R, Nakamura Y,**
787 **Berger F, Adam C, Aki SS, Althoff F, Araki T, Arteaga-Vazquez MA, Balasubrmanian S, Barry K,**
788 **Bauer D, Boehm CR, Briginshaw L, Caballero-Perez J, Catarino B, Chen F, Chiyoda S, Chovatia M,**
789 **Davies KM, Delmans M, Demura T, Dierschke T, Dolan L, Dorantes-Acosta AE, Eklund DM, Florent**
790 **SN, Flores-Sandoval E, Fujiyama A, Fukuzawa H, Galik B, Grimanelli D, Grimwood J, Grossniklaus**
791 **U, Hamada T, Haseloff J, Hetherington AJ, Higo A, Hirakawa Y, Hundley HN, Ikeda Y, Inoue K,**
792 **Inoue SI, Ishida S, Jia Q, Kakita M, Kanazawa T, Kawai Y, Kawashima T, Kennedy M, Kinose K,**
793 **Kinoshita T, Kohara Y, Koide E, Komatsu K, Kopischke S, Kubo M, Kyozuka J, Lagercrantz U, Lin**
794 **SS, Lindquist E, Lipzen AM, Lu CW, De Luna E, Martienssen RA, Minamino N, Mizutani M,**
795 **Mizutani M, Mochizuki N, Monte I, Mosher R, Nagasaki H, Nakagami H, Naramoto S, Nishitani K,**
796 **Ohtani M, Okamoto T, Okumura M, Phillips J, Pollak B, Reinders A, Rovekamp M, Sano R, Sawa**
797 **S, Schmid MW, Shirakawa M, Solano R, Spunde A, Suetsugu N, Sugano S, Sugiyama A, Sun R,**
798 **Suzuki Y, Takenaka M, Takezawa D, Tomogane H, Tsuzuki M, Ueda T, Umeda M, Ward JM,**
799 **Watanabe Y, Yazaki K, Yokoyama R, Yoshitake Y, Yotsui I, Zachgo S, Schmutz J** (2017) Insights
800 into land plant evolution garnered from the *Marchantia polymorpha* genome. Cell **171:** 287-304
801 e215

802 **Brown BA, Cloix C, Jiang GH, Kaiserli E, Herzyk P, Kliebenstein DJ, Jenkins GI** (2005) A UV-B-specific
803 signaling component orchestrates plant UV protection. Proc Natl Acad Sci USA **102:** 18225-18230

804 **Chen H, Huang X, Gusmaroli G, Terzaghi W, Lau OS, Yanagawa Y, Zhang Y, Li J, Lee JH, Zhu D, Deng XW**
805 (2010) Arabidopsis CULLIN4-damaged DNA binding protein 1 interacts with CONSTITUTIVELY
806 PHOTOMORPHOGENIC1-SUPPRESSOR OF PHYA complexes to regulate photomorphogenesis and
807 flowering time. Plant Cell **22:** 108-123

808 **Chiyoda S, Ishizaki K, Kataoka H, Yamato KT, Kohchi T** (2008) Direct transformation of the liverwort
809 *Marchantia polymorpha* L. by particle bombardment using immature thalli developing from spores.
810 Plant Cell Rep **27:** 1467-1473

811 **Christie JM, Arvai AS, Baxter KJ, Heilmann M, Pratt AJ, O'Hara A, Kelly SM, Hothorn M, Smith BO, Hitomi**
812 **K, Jenkins GI, Getzoff ED** (2012) Plant UVR8 photoreceptor senses UV-B by tryptophan-mediated
813 disruption of cross-dimer salt bridges. Science **335:** 1492-1496
814 **Clayton WA, Albert NW, Thrimawithana AH, McGhie TK, Deroles SC, Schwinn KE, Warren BA, McLachlan**
815 **ARG, Bowman JL, Jordan BR, Davies KM** (2018) UVR8-mediated induction of flavonoid
816 biosynthesis for UVB tolerance is conserved between the liverwort *Marchantia polymorpha* and
817 flowering plants. Plant J **96:** 503-517
818 **Cox J, Mann M** (2008) MaxQuant enables high peptide identification rates, individualized p.p.b.-range
819 mass accuracies and proteome-wide protein quantification. Nat Biotechnol **26:** 1367-1372
820 **Dannay M, Bertin C, Cavallari E, Albanese P, Tolleter D, Giustini C, Menneteau M, Brugiere S, Coute Y,**
821 **Finazzi G, Demarsy E, Ulm R, Allorent G** (2025) Photoreceptor-induced LHL4 protects the
822 photosystem II monomer in *Chlamydomonas reinhardtii*. Proc Natl Acad Sci USA **122:**
823 e2418687122
824 **Defossez E, Bourquin J, von Reuss S, Rasmann S, Glauser G** (2023) Eight key rules for successful data-
825 dependent acquisition in mass spectrometry-based metabolomics. Mass Spectrom Rev **42:** 131-
826 143
827 **Demarsy E, Goldschmidt-Clermont M, Ulm R** (2018) Coping with 'dark sides of the sun' through
828 photoreceptor signaling. Trends Plant Sci **23:** 260-271
829 **Dobin A, Davis CA, Schlesinger F, Drenkow J, Zaleski C, Jha S, Batut P, Chaisson M, Gingeras TR** (2013)
830 STAR: ultrafast universal RNA-seq aligner. Bioinformatics **29:** 15-21
831 **Duhrkop K, Fleischauer M, Ludwig M, Aksenov AA, Melnik AV, Meusel M, Dorrestein PC, Rousu J, Bocker**
832 **S** (2019) SIRIUS 4: a rapid tool for turning tandem mass spectra into metabolite structure
833 information. Nat Methods **16:** 299-302
834 **Fang F, Lin L, Zhang Q, Lu M, Skvortsova MY, Podolec R, Zhang Q, Pi J, Zhang C, Ulm R, Yin R** (2022)
835 Mechanisms of UV-B light-induced photoreceptor UVR8 nuclear localization dynamics. New Phytol
836 **236:** 1824-1837
837 **Favory JJ, Stec A, Gruber H, Rizzini L, Oravecz A, Funk M, Albert A, Cloix C, Jenkins GI, Oakeley EJ, Seidlitz**
838 **HK, Nagy F, Ulm R** (2009) Interaction of COP1 and UVR8 regulates UV-B-induced
839 photomorphogenesis and stress acclimation in Arabidopsis. EMBO J **28:** 591-601
840 **Findlay KM, Jenkins GI** (2016) Regulation of UVR8 photoreceptor dimer/monomer photo-equilibrium in
841 Arabidopsis plants grown under photoperiodic conditions. Plant Cell Environ **39:** 1706-1714
842 **Frangedakis E, Yelina NE, Billakurthi K, Hua L, Schreier T, Dickinson PJ, Tomaselli M, Haseloff J, Hibberd**
843 **JM** (2024) MYB-related transcription factors control chloroplast biogenesis. Cell **187:** 4859-4876
844 e4822
845 **Gabilly ST, Baker CR, Wakao S, Crisanto T, Guan K, Bi K, Guiet E, Guadagno CR, Niyogi KK** (2019)
846 Regulation of photoprotection gene expression in Chlamydomonas by a putative E3 ubiquitin
847 ligase complex and a homolog of CONSTANS. Proc Natl Acad Sci USA **116:** 17556-17562
848 **Gietz R, Smith J, Burke D** (2014) Yeast Genetics: Methods and Protocols.
849 **Gruber H, Heijde M, Heller W, Albert A, Seidlitz HK, Ulm R** (2010) Negative feedback regulation of UV-B-
850 induced photomorphogenesis and stress acclimation in Arabidopsis. Proc Natl Acad Sci USA **107:**
851 20132-20137
852 **Heijde M, Binkert M, Yin R, Ares-Orpel F, Rizzini L, Van De Slijke E, Persiau G, Nolf J, Gevaert K, De Jaeger**
853 **G, Ulm R** (2013) Constitutively active UVR8 photoreceptor variant in Arabidopsis. Proc Natl Acad
854 Sci USA **110:** 20326-20331
855 **Heijde M, Ulm R** (2013) Reversion of the Arabidopsis UV-B photoreceptor UVR8 to the homodimeric
856 ground state. Proc Natl Acad Sci USA **110:** 1113-1118
857 **Heilmann M, Jenkins GI** (2013) Rapid reversion from monomer to dimer regenerates the ultraviolet-B
858 photoreceptor UV RESISTANCE LOCUS8 in intact Arabidopsis plants. Plant Physiol **161:** 547-555

859 **Heilmann M, Velanis CN, Cloix C, Smith BO, Christie JM, Jenkins GI** (2016) Dimer/monomer status and in
860 vivo function of salt-bridge mutants of the plant UV-B photoreceptor UVR8. Plant J **88:** 71-81
861 **Hoecker U** (2017) The activities of the E3 ubiquitin ligase COP1/SPA, a key repressor in light signaling. Curr
862 Opin Plant Biol **37:** 63-69
863 **Holm M, Ma LG, Qu LJ, Deng XW** (2002) Two interacting bZIP proteins are direct targets of COP1-mediated
864 control of light-dependent gene expression in Arabidopsis. Genes Dev **16:** 1247-1259
865 **Hu S, Chen Y, Qian C, Ren H, Liang X, Tao W, Chen Y, Wang J, Dong Y, Han J, Ouyang X, Huang X** (2024)
866 Nuclear accumulation of rice UV-B photoreceptors is UV-B- and OsCOP1-independent for UV-B
867 responses. Nat Commun **15:** 6396
868 **Huang X, Ouyang X, Yang P, Lau OS, Chen L, Wei N, Deng XW** (2013) Conversion from CUL4-based COP1-
869 SPA E3 apparatus to UVR8-COP1-SPA complexes underlies a distinct biochemical function of COP1
870 under UV-B. Proc Natl Acad Sci USA **110:** 16669-16674
871 **Ishizaki K, Chiyoda S, Yamato KT, Kohchi T** (2008) Agrobacterium-mediated transformation of the haploid
872 liverwort *Marchantia polymorpha* L., an emerging model for plant biology. Plant Cell Physiol **49:**
873 1084-1091
874 **Kaiserli E, Jenkins GI** (2007) UV-B promotes rapid nuclear translocation of the Arabidopsis UV-B specific
875 signaling component UVR8 and activates its function in the nucleus. Plant Cell **19:** 2662-2673
876 **Kliebenstein DJ, Lim JE, Landry LG, Last RL** (2002) Arabidopsis UVR8 regulates ultraviolet-B signal
877 transduction and tolerance and contains sequence similarity to human regulator of chromatin
878 condensation 1. Plant Physiol **130:** 234-243
879 **Kondou Y, Miyagi Y, Morito T, Fujihira K, Miyauchi W, Moriyama A, Terasawa T, Ishida S, Iwabuchi K,**
880 **Kubo H, Nishihama R, Ishizaki K, Kohchi T** (2019) Physiological function of photoreceptor UVR8 in
881 UV-B tolerance in the liverwort *Marchantia polymorpha*. Planta **249:** 1349-1364
882 **Kreiss M, Haas FB, Hansen M, Rensing SA, Hoecker U** (2023) Co-action of COP1, SPA and cryptochrome in
883 light signal transduction and photomorphogenesis of the moss *Physcomitrium patens*. Plant J **114:**
884 159-175
885 **Kubota A, Ishizaki K, Hosaka M, Kohchi T** (2013) Efficient Agrobacterium-mediated transformation of the
886 liverwort *Marchantia polymorpha* using regenerating thalli. Biosci Biotechnol Biochem **77:** 167-
887 172
888 **Lau K, Podolec R, Chappuis R, Ulm R, Hothorn M** (2019) Plant photoreceptors and their signaling
889 components compete for COP1 binding via VP peptide motifs. EMBO J **38:** e102140
890 **Laubinger S, Fittinghoff K, Hoecker U** (2004) The SPA quartet: a family of WD-repeat proteins with a
891 central role in suppression of photomorphogenesis in arabidopsis. Plant Cell **16:** 2293-2306
892 **Leonardelli M, Tissot N, Podolec R, Ares-Orpel F, Glauser G, Ulm R, Demarsy E** (2024) Photoreceptor-
893 induced sinapate synthesis contributes to photoprotection in Arabidopsis. Plant Physiol **196:** 1518-
894 1533
895 **Li H, Li Y, Deng H, Sun X, Wang A, Tang X, Gao Y, Zhang N, Wang L, Yang S, Liu Y, Wang S** (2018) Tomato
896 UV-B receptor SlUVR8 mediates plant acclimation to UV-B radiation and enhances fruit chloroplast
897 development via regulating SlGLK2. Sci Rep **8:** 6097
898 **Li X, Ren H, Kundu M, Liu Z, Zhong FW, Wang L, Gao J, Zhong D** (2020) A leap in quantum efficiency
899 through light harvesting in photoreceptor UVR8. Nat Commun **11:** 4316
900 **Liang Y, Heyman J, Xiang Y, Vandendriessche W, Canher B, Goeminne G, De Veylder L** (2022) The wound-
901 activated ERF15 transcription factor drives *Marchantia polymorpha* regeneration by activating an
902 oxylipin biosynthesis feedback loop. Sci Adv **8:** eabo7737
903 **Liao Y, Smyth GK, Shi W** (2019) The R package Rsubread is easier, faster, cheaper and better for alignment
904 and quantification of RNA sequencing reads. Nucleic Acids Res **47:** e47

905 **Liu W, Giuriani G, Havlikova A, Li D, Lamont DJ, Neugart S, Velanis CN, Petersen J, Hoecker U, Christie**
906 **JM, Jenkins GI** (2024) Phosphorylation of Arabidopsis UVR8 photoreceptor modulates protein
907 interactions and responses to UV-B radiation. Nat Commun **15:** 1221
908 **Livak KJ, Schmittgen TD** (2001) Analysis of relative gene expression data using real-time quantitative PCR
909 and the 2(-Delta Delta C(T)) Method. Methods **25:** 402-408
910 **Love MI, Huber W, Anders S** (2014) Moderated estimation of fold change and dispersion for RNA-seq data
911 with DESeq2. Genome Biol **15:** 550
912 **Marrocco K, Zhou Y, Bury E, Dieterle M, Funk M, Genschik P, Krenz M, Stolpe T, Kretsch T** (2006)
913 Functional analysis of EID1, an F-box protein involved in phytochrome A-dependent light signal
914 transduction. Plant J **45:** 423-438
915 **McNellis TW, von Arnim AG, Araki T, Komeda Y, Misera S, Deng XW** (1994) Genetic and molecular analysis
916 of an allelic series of *cop1* mutants suggests functional roles for the multiple protein domains.
917 Plant Cell **6:** 487-500
918 **Messant M, Hani U, Hennebelle T, Guerard F, Gakiere B, Gall A, Thomine S, Krieger-Liszkay A** (2023)
919 Manganese concentration affects chloroplast structure and the photosynthetic apparatus in
920 *Marchantia polymorpha*. Plant Physiol **192:** 356-369
921 **Moriconi V, Binkert M, Costigliolo C, Sellaro R, Ulm R, Casal JJ** (2018) Perception of sunflecks by the UV-
922 B photoreceptor UV RESISTANCE LOCUS8. Plant Physiol **177:** 75-81
923 **Mulvey H, Dolan L** (2023) RHO GTPase of plants regulates polarized cell growth and cell division
924 orientation during morphogenesis. Curr Biol **33:** 2897-2911 e2896
925 **Murchie EH, Lawson T** (2013) Chlorophyll fluorescence analysis: a guide to good practice and
926 understanding some new applications. J Exp Bot **64:** 3983-3998
927 **Oravecz A, Baumann A, Mate Z, Brzezinska A, Molinier J, Oakeley EJ, Adam E, Schafer E, Nagy F, Ulm R**
928 (2006) CONSTITUTIVELY PHOTOMORPHOGENIC1 is required for the UV-B response in Arabidopsis.
929 Plant Cell **18:** 1975-1990
930 **Ordonez-Herrera N, Fackendahl P, Yu X, Schaefer S, Koncz C, Hoecker U** (2015) A *cop1 spa* mutant
931 deficient in COP1 and SPA proteins reveals partial co-action of COP1 and SPA during Arabidopsis
932 post-embryonic development and photomorphogenesis. Mol Plant **8:** 479-481
933 **Pham VN, Paik I, Hoecker U, Huq E** (2020) Genomic evidence reveals SPA-regulated developmental and
934 metabolic pathways in dark-grown Arabidopsis seedlings. Physiol Plant **169:** 380-396
935 **Podolec R, Demarsy E, Ulm R** (2021a) Perception and signaling of ultraviolet-B radiation in plants. Annu
936 Rev Plant Biol **72:** 793-822
937 **Podolec R, Lau K, Wagnon TB, Hothorn M, Ulm R** (2021b) A constitutively monomeric UVR8 photoreceptor
938 confers enhanced UV-B photomorphogenesis. Proc Natl Acad Sci USA **118:** e2017284118
939 **Podolec R, Ulm R** (2018) Photoreceptor-mediated regulation of the COP1/SPA E3 ubiquitin ligase. Curr
940 Opin Plant Biol **45:** 18-25
941 **Ponnu J, Hoecker U** (2021) Illuminating the COP1/SPA ubiquitin ligase: fresh insights into its structure and
942 functions during plant photomorphogenesis. Front Plant Sci **12:** 662793
943 **Ponnu J, Riedel T, Penner E, Schrader A, Hoecker U** (2019) Cryptochrome 2 competes with COP1
944 substrates to repress COP1 ubiquitin ligase activity during Arabidopsis photomorphogenesis. Proc
945 Natl Acad Sci USA **116:** 27133-27141
946 **Qian C, Chen Z, Liu Q, Mao W, Chen Y, Tian W, Liu Y, Han J, Ouyang X, Huang X** (2020) Coordinated
947 transcriptional regulation by the UV-B photoreceptor and multiple transcription factors for plant
948 UV-B responses. Mol Plant **13:** 777-792
949 **Rai N, Neugart S, Yan Y, Wang F, Siipola SM, Lindfors AV, Winkler JB, Albert A, Brosche M, Lehto T,**
950 **Morales LO, Aphalo PJ** (2019) How do cryptochromes and UVR8 interact in natural and simulated
951 sunlight? J Exp Bot **70:** 4975-4990

952 **Ranjan A, Dickopf S, Ullrich KK, Rensing SA, Hoecker U** (2014) Functional analysis of COP1 and SPA
953 orthologs from Physcomitrella and rice during photomorphogenesis of transgenic Arabidopsis
954 reveals distinct evolutionary conservation. BMC Plant Biol **14:** 178
955 **Rappsilber J, Ishihama Y, Mann M** (2003) Stop and go extraction tips for matrix-assisted laser
956 desorption/ionization, nanoelectrospray, and LC/MS sample pretreatment in proteomics. Anal
957 Chem **75:** 663-670
958 **Rizzini L, Favory JJ, Cloix C, Faggionato D, O'Hara A, Kaiserli E, Baumeister R, Schafer E, Nagy F, Jenkins**
959 **GI, Ulm R** (2011) Perception of UV-B by the Arabidopsis UVR8 protein. Science **332:** 103-106
960 **Rutz A, Allard P** (2025) tima: Taxonomically Informed Metabolite Annotation (2.11.0) [R package]. Zenodo**:**
961 https://doi.org/10.5281/zenodo.5797920
962 **Saint-Marcoux D, Proust H, Dolan L, Langdale JA** (2015) Identification of reference genes for real-time
963 quantitative PCR experiments in the liverwort *Marchantia polymorpha*. PLoS One **10:** e0118678
964 **Sauret-Güeto S, Frangedakis E, Silvestri L, Rebmann M, Tomaselli M, Markel K, Delmans M, West A,**
965 **Patron NJ, Haseloff J** (2020) Systematic tools for reprogramming plant gene expression in a simple
966 model, *Marchantia polymorpha*. ACS Synth Biol **9:** 864-882
967 **Sawano A, Miyawaki A** (2000) Directed evolution of green fluorescent protein by a new versatile PCR
968 strategy for site-directed and semi-random mutagenesis. Nucleic Acids Res **28:** E78
969 **Schmid R, Heuckeroth S, Korf A, Smirnov A, Myers O, Dyrlund TS, Bushuiev R, Murray KJ, Hoffmann N,**
970 **Lu M, Sarvepalli A, Zhang Z, Fleischauer M, Duhrkop K, Wesner M, Hoogstra SJ, Rudt E, Mokshyna**
971 **O, Brungs C, Ponomarov K, Mutabdzija L, Damiani T, Pudney CJ, Earll M, Helmer PO, Fallon TR,**
972 **Schulze T, Rivas-Ubach A, Bilbao A, Richter H, Nothias LF, Wang M, Oresic M, Weng JK, Bocker S,**
973 **Jeibmann A, Hayen H, Karst U, Dorrestein PC, Petras D, Du X, Pluskal T** (2023) Integrative analysis
974 of multimodal mass spectrometry data in MZmine 3. Nat Biotechnol **41:** 447-449
975 **Soriano G, Cloix C, Heilmann M, Nunez-Olivera E, Martinez-Abaigar J, Jenkins GI** (2018) Evolutionary
976 conservation of structure and function of the UVR8 photoreceptor from the liverwort *Marchantia*
977 *polymorpha* and the moss *Physcomitrella patens*. New Phytol **217:** 151-162
978 **Soriano G, Del-Castillo-Alonso MA, Monforte L, Nunez-Olivera E, Martinez-Abaigar J** (2019) Acclimation
979 of bryophytes to sun conditions, in comparison to shade conditions, is influenced by both
980 photosynthetic and ultraviolet radiations. Front Plant Sci **10:** 998
981 **Stelzl U, Worm U, Lalowski M, Haenig C, Brembeck FH, Goehler H, Stroedicke M, Zenkner M, Schoenherr**
982 **A, Koeppen S, Timm J, Mintzlaff S, Abraham C, Bock N, Kietzmann S, Goedde A, Toksoz E, Droege**
983 **A, Krobitsch S, Korn B, Birchmeier W, Lehrach H, Wanker EE** (2005) A human protein-protein
984 interaction network: a resource for annotating the proteome. Cell **122:** 957-968
985 **Stockenhuber R, Akiyama R, Tissot N, Milosavljevic S, Yamazaki M, Wyler M, Arongaus AB, Podolec R,**
986 **Sato Y, Widmer A, Ulm R, Shimizu KK** (2024) UV RESISTANCE LOCUS 8-mediated UV-B response is
987 required alongside CRYPTOCHROME 1 for plant survival in sunlight under field conditions. Plant
988 Cell Physiol **65:** 35-48
989 **Stracke R, Favory JJ, Gruber H, Bartelniewoehner L, Bartels S, Binkert M, Funk M, Weisshaar B, Ulm R**
990 (2010) The Arabidopsis bZIP transcription factor HY5 regulates expression of the *PFG1*/*MYB12*
991 gene in response to light and ultraviolet-B radiation. Plant Cell Environ **33:** 88-103
992 **Sugano SS, Nishihama R, Shirakawa M, Takagi J, Matsuda Y, Ishida S, Shimada T, Hara-Nishimura I,**
993 **Osakabe K, Kohchi T** (2018) Efficient CRISPR/Cas9-based genome editing and its application to
994 conditional genetic analysis in *Marchantia polymorpha*. PLoS One **13:** e0205117
995 **Tavridou E, Pireyre M, Ulm R** (2020a) Degradation of the transcription factors PIF4 and PIF5 under UV-B
996 promotes UVR8-mediated inhibition of hypocotyl growth in Arabidopsis. Plant J **101:** 507-517
997 **Tavridou E, Schmid-Siegert E, Fankhauser C, Ulm R** (2020b) UVR8-mediated inhibition of shade avoidance
998 involves HFR1 stabilization in Arabidopsis. PLoS Genet **16:** e1008797

Tilbrook K, Dubois M, Crocco CD, Yin R, Chappuis R, Allorent G, Schmid-Siegert E, Goldschmidt-Clermont M, Ulm R (2016) UV-B perception and acclimation in *Chlamydomonas reinhardtii*. Plant Cell **28:** 966-983

Tokutsu R, Fujimura-Kamada K, Matsuo T, Yamasaki T, Minagawa J (2019) The CONSTANS flowering complex controls the protective response of photosynthesis in the green alga Chlamydomonas. Nat Commun **10:** 4099

Trimborn L, Kuttig F, Ponnu J, Yu P, Korsching KR, Lederer P, Urquiza-Garcia U, Zurbriggen MD, Hoecker U (2025) Cryptochrome 1 promotes photomorphogenesis in Arabidopsis by displacing substrates from the COP1 ubiquitin ligase. Plant J **121:** e70071

Tyanova S, Temu T, Cox J (2016) The MaxQuant computational platform for mass spectrometry-based shotgun proteomics. Nat Protoc **11:** 2301-2319

Ulm R, Baumann A, Oravecz A, Mate Z, Adam E, Oakeley EJ, Schafer E, Nagy F (2004) Genome-wide analysis of gene expression reveals function of the bZIP transcription factor HY5 in the UV-B response of Arabidopsis. Proc Natl Acad Sci USA **101:** 1397-1402

Wang L, Wang Y, Chang H, Ren H, Wu X, Wen J, Guan Z, Ma L, Qiu L, Yan J, Zhang D, Huang X, Yin P (2023) RUP2 facilitates UVR8 redimerization via two interfaces. Plant Commun **4:** 100428

Wang W, Paik I, Kim J, Hou X, Sung S, Huq E (2021) Direct phosphorylation of HY5 by SPA kinases to regulate photomorphogenesis in Arabidopsis. New Phytol **230:** 2311-2326

Wang Y, Wang L, Guan Z, Chang H, Ma L, Shen C, Qiu L, Yan J, Zhang D, Li J, Deng XW, Yin P (2022) Structural insight into UV-B-activated UVR8 bound to COP1. Sci Adv **8:** eabn3337

Wu D, Hu Q, Yan Z, Chen W, Yan C, Huang X, Zhang J, Yang P, Deng H, Wang J, Deng X, Shi Y (2012) Structural basis of ultraviolet-B perception by UVR8. Nature **484:** 214-219

Yelina NE, Frangedakis E, Wang Z, Schreier TB, Rever J, Tomaselli M, Forestier ECF, Billakurthi K, Ren S, Bai Y, Stewart-Wood J, Haseloff J, Zhong S, Hibberd JM (2024) Streamlined regulation of chloroplast development in the liverwort *Marchantia polymorpha*. Cell Rep **43:** 114696

Yin R, Arongaus AB, Binkert M, Ulm R (2015) Two distinct domains of the UVR8 photoreceptor interact with COP1 to initiate UV-B signaling in Arabidopsis. Plant Cell **27:** 202-213

Yin R, Skvortsova MY, Loubery S, Ulm R (2016) COP1 is required for UV-B-induced nuclear accumulation of the UVR8 photoreceptor. Proc Natl Acad Sci USA **113:** E4415-4422

Zhang L, Li T, Su S, Peng H, Li S, Li K, Ji L, Xing Y, Zhang J, Du X, Bian M, Liao Y, Yang Z, Zuo Z (2021) Functions of COP1/SPA E3 ubiquitin ligase mediated by MpCRY in the liverwort *Marchantia polymorpha* under blue light. Int J Mol Sci **23:** 158

Zhou Z, Bi G, Zhou JM (2018) Luciferase complementation assay for protein-protein interactions in plants. Curr Protoc Plant Biol **3:** 42-50

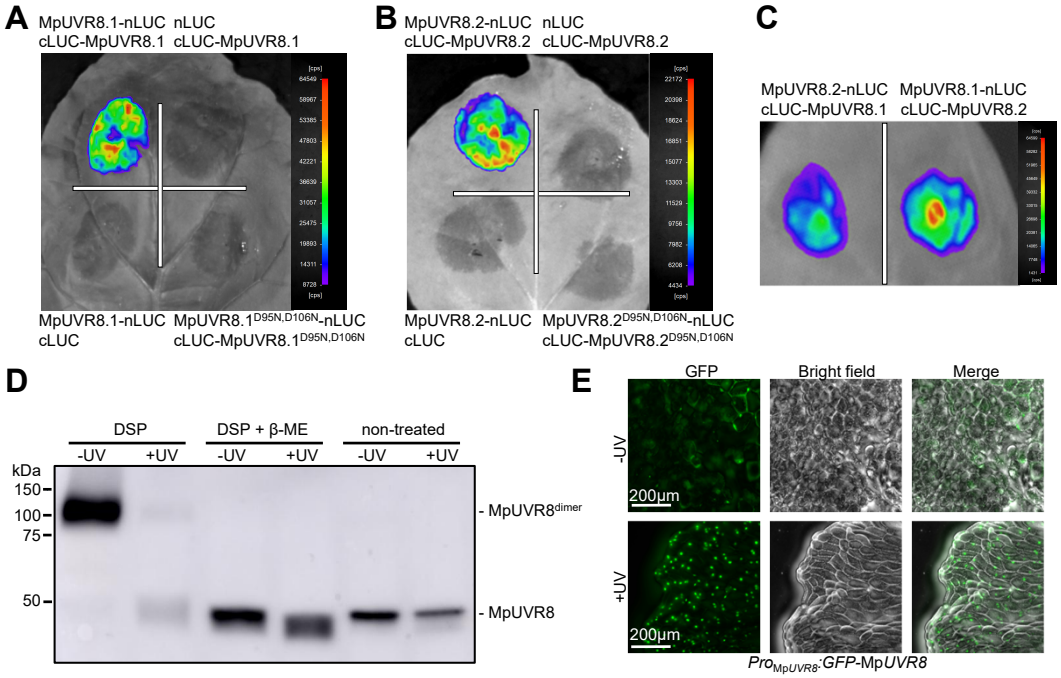

Figure 1. MpUVR8.1 and MpUVR8.2 form dimers in their ground state, monomerize upon UV-B exposure, and accumulate in the nucleus. **A-C)** Luciferase complementation imaging (LCI) assays assessing monomer interaction for MpUVR8.1 (A) and MpUVR8.2 (B), as well as their D95N,D106N variants, and MpUVR8.1 and MpUVR8.2 (C). MpUVR8 versions were fused to N-terminal (nLUC) or C-terminal (cLUC) fragments of luciferase, expressed in *N. benthamiana* leaves and imaged 2 days after infiltration. An image of a representative leaf is shown. Cps, counts per second. **D)** Immunoblot analysis of MpUVR8 dimer/monomer levels in 7-day-old wild type (Tak-1) gemmalings irradiated (+UV) or not (-UV) for 20 min with broadband UV-B. Protein extracts were either crosslinked with DSP, DSP crosslinked then reversed with the reducing agent β-mercaptoethanol (DSP + β-ME), or non-treated. **E)** Subcellular localization of GFP-MpUVR8 in 7-day-old gemmalings of a Tak-1/*Pro*$_{\text{MpUVR8}}$*:GFP*-Mp*UVR8* line, grown in white light and irradiated or not for 20 min with 25 µmol m^{-2} s^{-1} broadband UV-B (+UV and -UV, respectively). Bars = 200 µm.

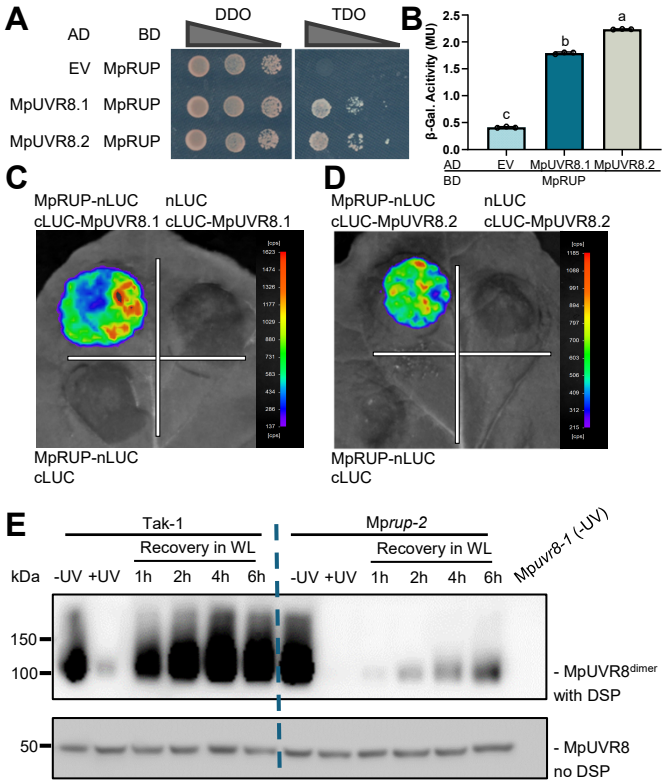

Figure 2. MpRUP facilitates MpUVR8 redimerization. **A)** Yeast two-hybrid assays of MpUVR8.1 and MpUVR8.2 interactions with MpRUP. Representative images of serial dilutions spotted on non-selective SD/-Trp/-Leu double dropout (DDO) and selective SD/-Trp/-Leu/-His triple dropout (TDO) media are shown. AD, transcriptional activation domain; BD, DNA-binding domain; EV, empty vector. **B)** Quantitative yeast two-hybrid assays of MpUVR8.1 and MpUVR8.2 interactions with MpRUP. Individual data points of biological replicates and means ± SD are shown (n = 3). Different letters indicate statistically significant differences between the means ($P < 0.01$) as determined by one-way ANOVA followed by Tukey's post hoc honestly significant difference (HSD) test. β-Gal., β-galactosidase; MU, Miller units. **C** and **D)** LCI assays of MpRUP interactions with MpUVR8.1 (C) and MpUVR8.2 (D) fused to N-terminal (nLUC) or C-terminal (cLUC) luciferase fragments, expressed in *N. benthamiana* leaves and imaged 2 days after infiltration. Images of representative leaves are shown. Cps, counts per second. **E)** Immunoblot analysis of MpUVR8 levels in 7-day-old wild type (Tak-1) and Mp*rup-2* gemmalings irradiated for 20 min with broadband UV-B (+UV) before recovery in white light (WL) for the indicated times (1–6 h). Non-irradiated samples (-UV) are included as MpUVR8 ground state controls alongside a negative control -UV Mp*uvr8-1* sample. Top: MpUVR8 dimer levels in DSP-crosslinked protein extracts; bottom: total MpUVR8 levels in non-crosslinked extracts.

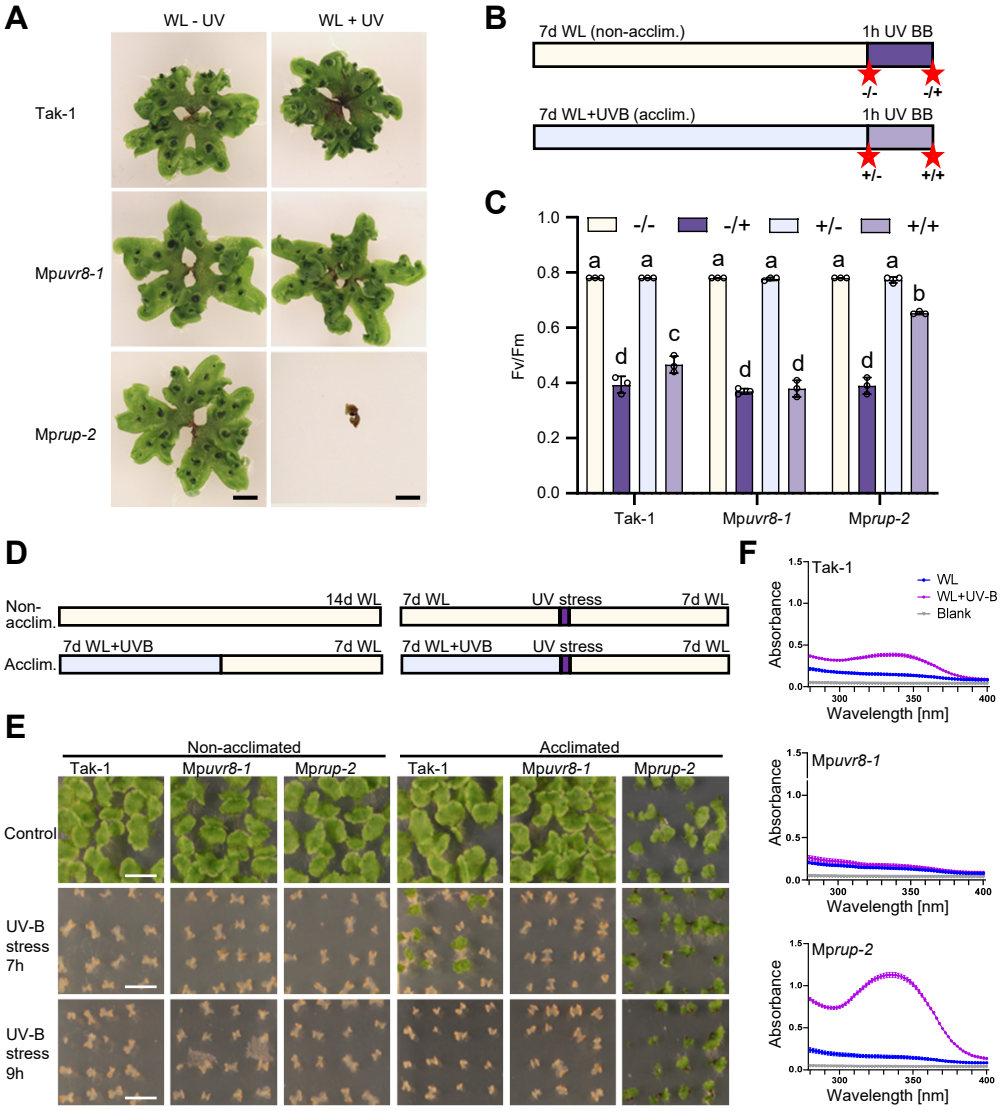

Figure 3. UV-B acclimation and survival is impaired in Mp*uvr8* and enhanced in Mp*rup*. **A)** Growth phenotype of 4-week-old wild-type (Tak-1), Mp*uvr8-1*, and Mp*rup-2* grown in white light supplemented (WL+UV) or not (WL-UV) with UV-B (1.5 µmol m^{-2} s^{-1}). Bars = 1 cm. **B)** Scheme for UV-B treatment and sampling for F_v/F_m measurements. Light yellow bar: white light (WL, 50 µmol m^{-2} s^{-1}), non-acclimated condition; light blue bar: white light supplemented with narrowband UV-B (WL+UVB, 1.5 µmol m^{-2} s^{-1}), acclimated condition; light/dark purple bars: broadband UV stress (UV BB, 25 µmol m^{-2} s^{-1}). Red stars indicate timepoints of measurements: -/-, non-acclimated, non-stressed; -/+, non-acclimated, stressed; +/-, acclimated, non-stressed; +/+, acclimated, stressed. **C)** F_v/F_m in 7-day-old wild-type (Tak-1), Mp*uvr8-1*, and Mp*rup-2* gemmalings grown and sampled as indicated in (B). Individual data points of biological replicates and means ± SD are shown (n = 3). Different letters indicate statistically significant differences between the means ($P < 0.01$) as determined by two-way ANOVA followed by Tukey's post hoc honestly significant difference (HSD) test. **D)** Scheme for UV-B stress survival experiments. Plants were grown in WL or WL+UVB for 7 days, then exposed to 7 or 9 h of broadband UV-B stress, followed by recovery for 7 days in WL, after which they were imaged. **E)** UV-B stress survival in Tak-1, Mp*uvr8-1*, and Mp*rup-2* gemmalings grown as indicated in (D). Representative images are shown; bars = 1 cm. **F)** Absorbance spectra (280–400 nm) of methanolic extracts from 9-day-old Tak-1, Mp*uvr8-1*, and Mp*rup-2* gemmalings grown for 7 days in white light and exposed (WL+UV-B, purple lines) or not (WL, blue lines) to supplemental UV-B (1.5 µmol m^{-2} s^{-1}) for 2 days. The gray line shows the absorbance of the buffer (blank). Values of independent measurements and means ± SEM are shown (n = 3).

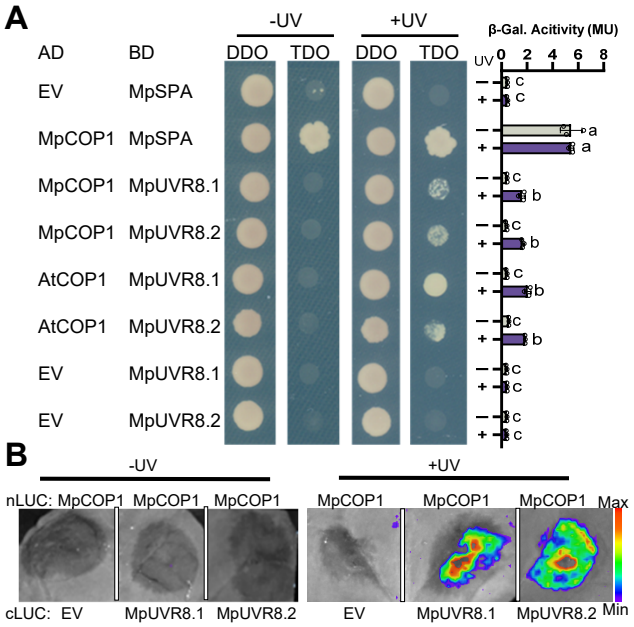

Figure 4. MpUVR8 and MpCOP1 interact in a UV-B-dependent manner. **A)** Yeast two-hybrid assay of the interactions of MpCOP1 with MpSPA and MpUVR8, as well as AtCOP1 with MpUVR8, in the presence (+UV) or absence (-UV) of UV-B. Left, growth assay; right, quantitative assay. Yeasts were grown on non-selective SD/-Trp/-Leu (DDO) or selective SD /-Trp/-Leu/-His (TDO) media. Individual data points of biological replicates and means ± SD are shown (n = 3). Different letters indicate statistically significant differences between the means ($P < 0.01$) as determined by one-way ANOVA followed by Tukey's post hoc honestly significant difference (HSD) test. AD, Gal4 activation domain; BD, LexA DNA-binding domain; β-Gal., β-galactosidase; MU, Miller units; EV, empty vector. **B)** LCI assays of MpCOP1 with MpUVR8.1 and MpUVR8.2. N-terminal (nLUC) or C-terminal (cLUC) luciferase fusion proteins were expressed in *N. benthamiana* leaves and imaged 2 days after infiltration, with (+UV) or without (-UV) exposure to 20 min of broadband UV-B. An image of a representative leaf is shown.

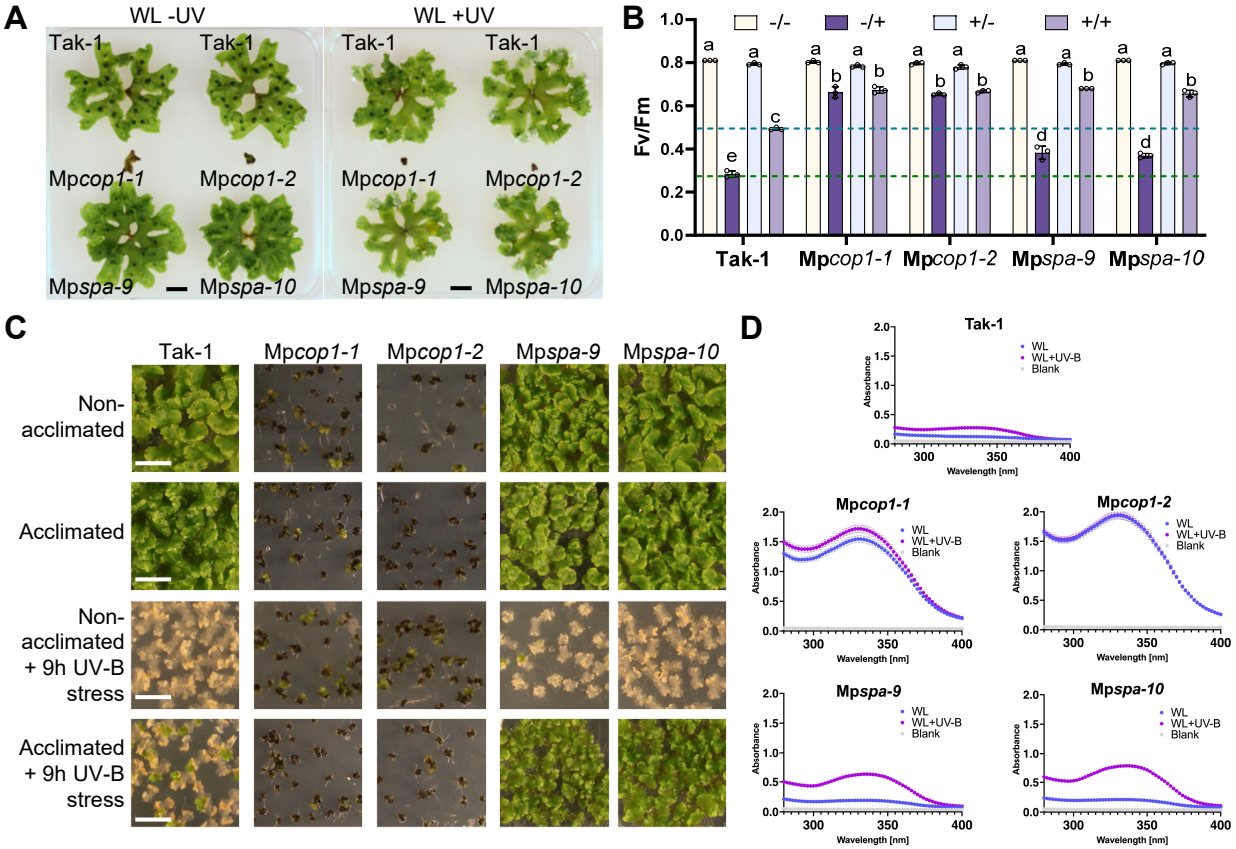

Figure 5. Mp*cop1* shows constitutive photomorphogenesis and UV-B tolerance, whereas Mp*spa* shows enhanced UV-B-induced UV-B tolerance. **A)** Growth phenotype of 4-week-old wild-type (Tak-1), Mp*cop1-1*, Mp*cop1-2*, Mp*spa-9*, and Mp*spa-10* plants grown in white light supplemented (WL +UV) or not (WL -UV) with UV-B. Scale bars = 1 cm. **B)** F_v/F_m measurements in 7-day-old wild-type (Tak-1), Mp*cop1-1*, *Mpcop1-2*, Mp*spa-9*, and Mp*spa-10* gemmalings grown in white light (non-acclimated) or white light supplemented with UV-B (acclimated), without (non-stressed) or with (stressed) additional exposure to broadband UV-B stress for 60 min. -/-, non-acclimated, non-stressed; -/+, non-acclimated, stressed; +/-, acclimated, non-stressed; +/+, acclimated, stressed. Individual data points of biological replicates and means ± SD are shown (n = 3). Different letters indicate statistically significant differences between the means ($P < 0.01$) as determined by two-way ANOVA followed by Tukey's post hoc honestly significant difference (HSD) test. **C)** UV-B stress survival in wild-type (Tak-1), Mp*cop1-1*, Mp*cop1-2*, Mp*spa-9*, and Mp*spa-10* plants grown for 7 days in white light supplemented (acclimated) or not (non-acclimated) with UV-B, then exposed or not to 9 h of broadband UV-B stress. Pictures were taken after a further 7-day recovery period in white light. **D)** Absorbance spectra (280–400 nm) of methanolic extracts from 9-day-old wild-type (Tak-1), Mp*cop1-1,* Mp*cop1-2*, Mp*spa-9*, and Mp*spa-10* gemmalings grown for 7 days in white light supplemented (WL+UV-B, purple lines) or not (WL, blue lines) with UV-B. The gray line shows the absorbance of the buffer (blank). Values of independent measurements and means ± SEM are shown (n = 3).

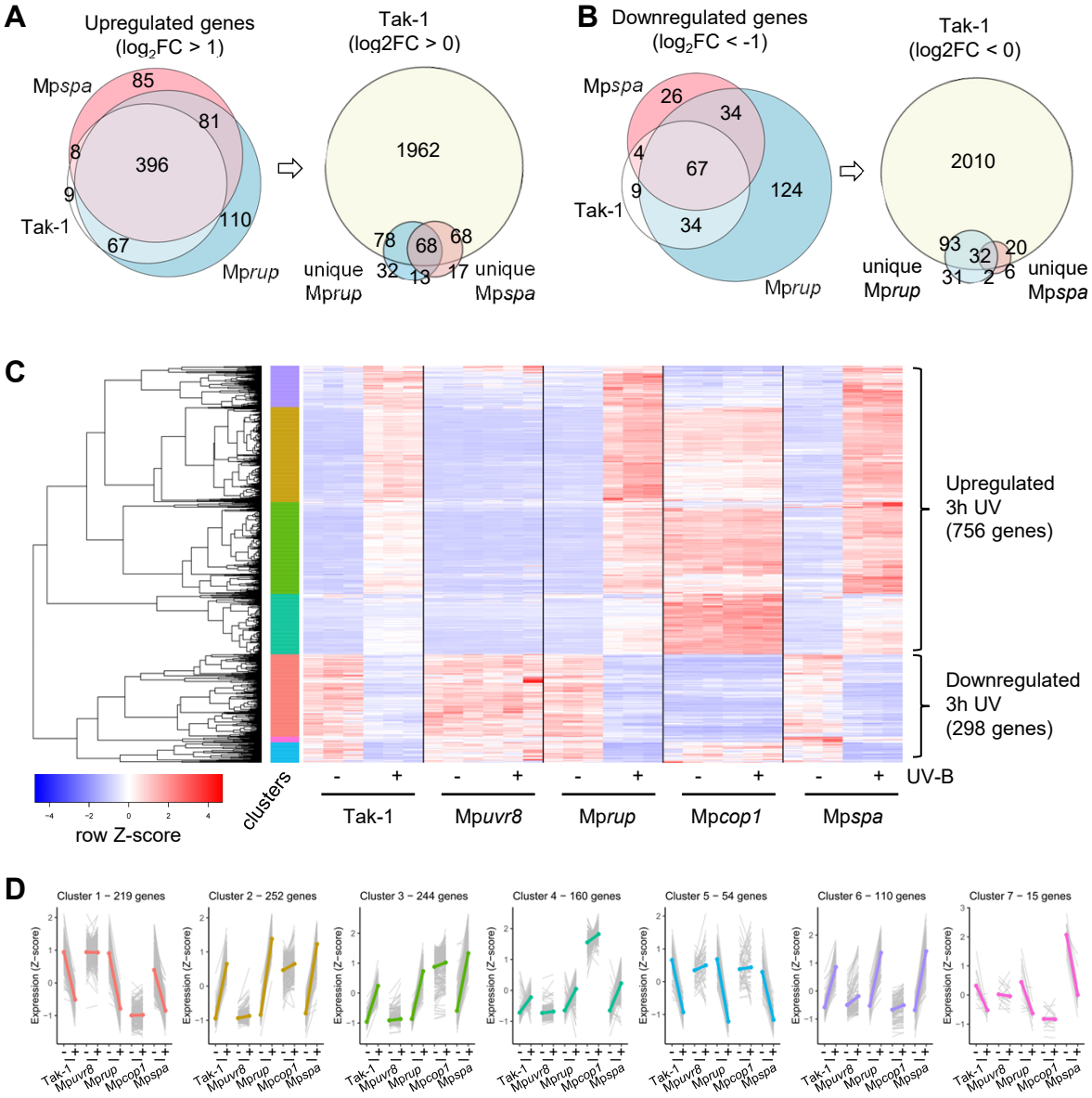

Figure 6. Transcriptome analysis reveals MpUVR8- and MpCOP1-dependent, UV-B-responsive gene regulation that is repressed by MpRUP and MpSPA. **A)** Euler plots showing overlaps between upregulated differentially expressed genes (DEGs) (p-adj < 0.05) upon exposure to 3 h UV-B in 7-day-old wild-type (Tak-1), Mp*rup*, and Mp*spa* gemmalings. Left: overlap between genes upregulated at least two-fold ($log_2FC > 1$) in either Tak-1, Mp*rup*, or Mp*spa*. Right: overlap between upregulated ($log_2FC > 1$) genes that are unique to Mp*rup* and/or Mp*spa*, and Tak-1 upregulated genes without a fold-change threshold ($log_2FC > 0$). Corresponding gene lists: table S3a. **B)** Euler plots showing overlaps between downregulated DEGs (p-adj < 0.05) upon exposure to 3 h UV-B in 7-day-old Tak-1, Mp*rup*, and Mp*spa* gemmalings. Left: overlap between genes downregulated at least two-fold ($log_2FC < -1$) in either Tak-1, Mp*rup*, or Mp*spa*. Right: overlap between downregulated ($log_2FC < -1$) genes that are unique to Mp*rup* and/or Mp*spa*, and Tak-1 downregulated genes without a fold-change threshold ($log_2FC < 0$). Corresponding gene lists: table S3b. **C)** Hierarchical clustering and heatmap of UV-B-regulated gene expression in Tak-1, Mp*uvr8-1,* Mp*rup-2,* Mp*cop1-1*, and Mp*spa-9* plants grown for 7 days under white light and exposed or not to supplemental UV-B for 3 h. All genes with a greater than two-fold change in expression in response to UV-B and a p-adj < 0.05 in at least one genotype are shown (total = 1005 genes). Red and blue colors indicate normalized read count Z-scores. The color bar on the left side indicates 7 major profiles (clusters) of gene expression. **D)** Gene expression profiles in clusters identified by hierarchical clustering. Z-scores for normalized read count values for each gene (gray lines) and for the cluster average (colored line) are shown.

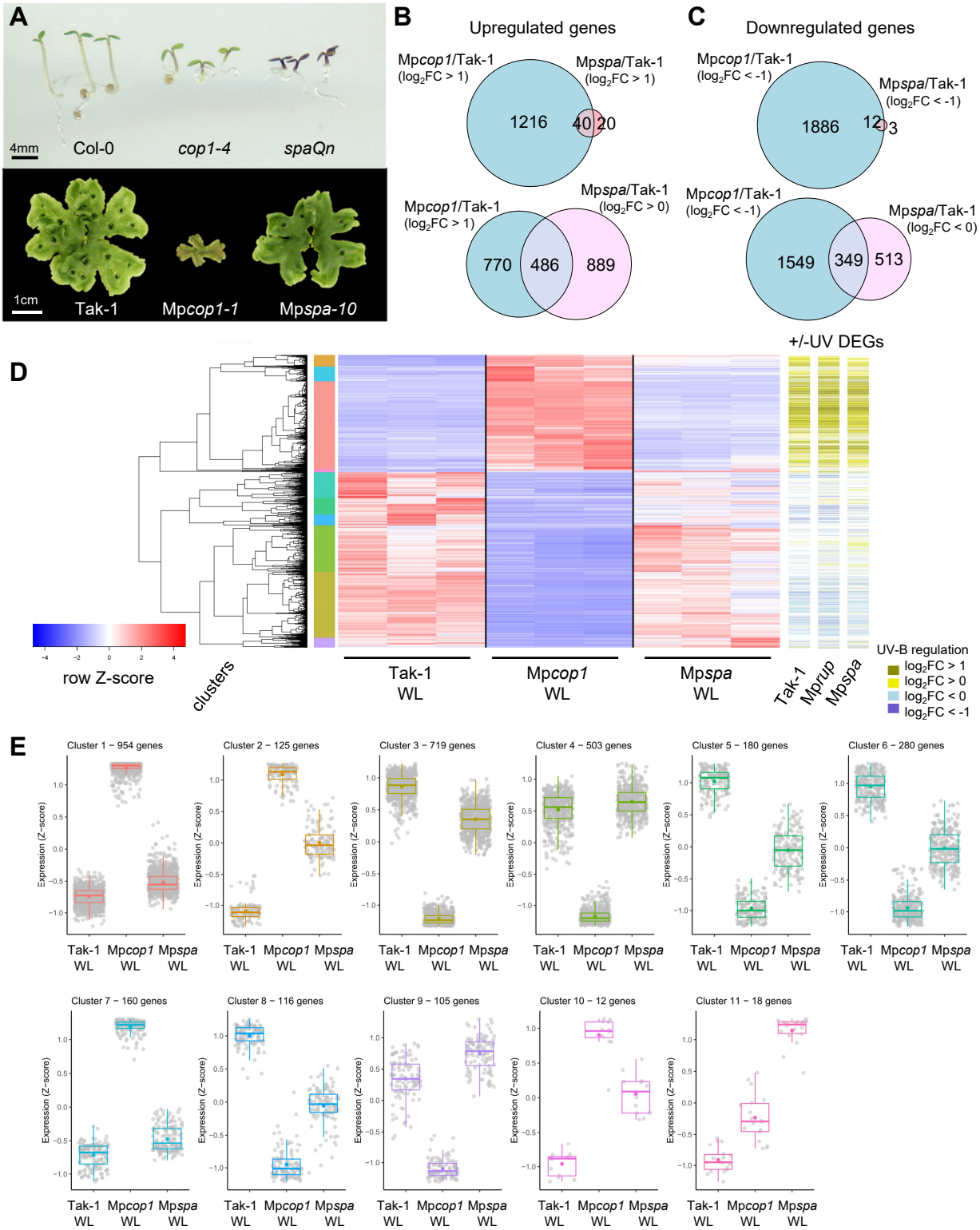

Figure 7. MpSPA plays a minor role in repressing Marchantia photomorphogenesis under visible light. **A)** Representative images of 4-day-old Arabidopsis seedlings of wild-type (Col-0), *cop1-4*, and *spaQn* mutants, and 28-day-old Marchantia thalli of wild-type (Tak-1), Mp*cop1-1*, and Mp*spa-10* grown in white light. Scale bars: 4 mm or 1 cm, as indicated. **B)** Euler plots showing overlaps between upregulated DEGs (p-adj < 0.05) in Mp*cop1* and Mp*spa* mutants compared to Tak-1 wild type. Gemmalings were grown for 7 days in white light. Top: overlap between genes upregulated at least two-fold ($log_2FC > 1$) in either Mp*cop1*/Tak-1 or Mp*spa*/Tak-1. Bottom: overlap between genes upregulated at least two-fold ($log_2FC > 1$) in Mp*cop1*/Tak-1 and genes upregulated without a fold-change threshold ($log_2FC > 0$) in Mp*spa*/Tak-1. Corresponding gene lists: table S3c. **C)** Euler plots showing overlaps between downregulated DEGs (p-adj < 0.05) in Mp*cop1* and Mp*spa* mutants compared to Tak-1 wild type. Gemmalings were grown for 7 days in white light. Top: overlap between genes downregulated at least two-fold ($log_2FC < -1$) in either Mp*cop1*/Tak-1 or Mp*spa*/Tak-1. Bottom: overlap between genes downregulated at least two-fold ($log_2FC < -1$) in Mp*cop1*/Tak-1 and genes downregulated without a fold-change threshold ($log_2FC < 0$) in Mp*spa*/Tak-1. Corresponding gene lists: table S3d. **D)** Hierarchical clustering and heatmap of gene expression in Tak-1, Mp*cop1-1*, and Mp*spa-9* plants grown for 7 days in white light. All genes with a greater than two-fold change in expression between mutants and wild type and a p-adj < 0.05 in at least one comparison are shown (total = 2975 genes). Red and blue colors indicate normalized read count Z-scores. The color bar on the left side indicates 11 major profiles (clusters) of gene expression. The color bars on the right indicate if genes are significantly regulated after UV-B exposure in Tak-1, Mp*rup*, and Mp*spa*. **E)** Gene expression profiles in clusters identified by hierarchical clustering. Z-scores for normalized read count values for each gene are shown as gray points; their distribution is represented as a colored box plot.

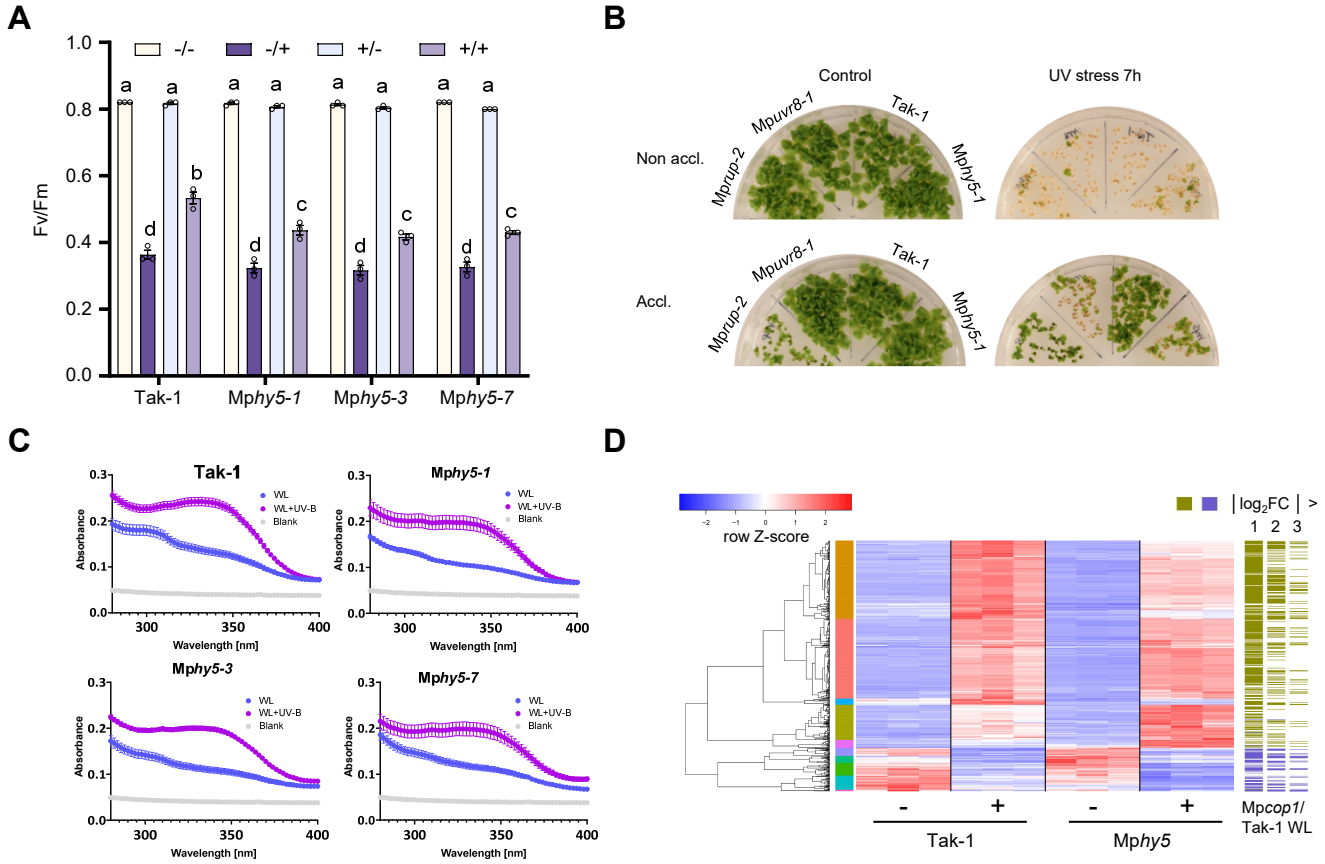

Figure 8. MpHY5 is involved in UV-B and visible light photomorphogenesis. **A)** F_v/F_m measurements in wild-type (Tak-1), Mp*hy5-1*, Mp*hy5-3*, and Mp*hy5-7* plants grown for 7 days in white light (non-acclimated) or white light supplemented with UV-B (acclimated), without (not stressed) or with (stressed) additional exposure to broadband UV-B stress for 60 min. -/-, not acclimated, not stressed; -/+, not acclimated, stressed; +/-, acclimated, not stressed; +/+, acclimated, stressed. Individual data points of biological replicates and means ± SD are shown (*n* = 3). Letters indicate statistically significant differences between the means (P < 0.01) as determined by two-way ANOVA followed by Tukey's post hoc honestly significant difference (HSD) test. **B)** UV-B stress survival of Tak-1, Mp*hy5-1*, Mp*rup-2*, and Mp*uvr8-1* plants grown for 7 days in white light supplemented (Accl.) or not (Non-accl.) with UV-B, then exposed to 7 h of broadband UV-B stress (UV stress 7h) or not (Control). Pictures were taken after recovery for another 7 days in white light. **C)** Absorbance spectra (280–400 nm) of methanolic extracts from 9-day-old Tak-1, Mp*hy5-1*, Mp*hy5-3*, and Mp*hy5-7* gemmalings grown for 7 days in white light and exposed (WL+UV-B, purple lines) or not (WL, blue lines) to supplemental UV-B (1.5 µmol m^{-2} s^{-1}) for 2 days. The gray lines show absorbance of the buffer (blank). Values of independent measurements and means ± SEM are shown (*n* = 3). **D)** Hierarchical clustering and heatmap of UV-B-regulated gene expression in Tak-1 and Mp*hy5-1* plants grown for 7 days and exposed, or not, to supplemental UV-B for 3h. All genes with a greater than two-fold change in expression under UV-B and a p-adj < 0.05 in at least one genotype are shown (total = 501 genes). Red and blue colors indicate normalized read count Z-scores. The color bar on the left side indicates 10 major profiles (clusters) of gene expression. The color bars on the right indicate if genes are significantly misregulated in white light in Mp*cop1* compared to Tak-1, at varying fold-change thresholds.

```
AtUVR8      1 MAEDMAADEVTAPPRKVLIISAGASHSVALLSGDIVCSWGRGEDGQLGHGDAEDRPSPTQ  60
MpUVR8.1    1 -MEDSKMSSNERPRRRVLFVSAGASHSVALLTGDSVCSWGRGEDGQLGHGDADERHLPTI  59
MpUVR8.2    1 -MEDSKMSSNERPRRRVLFVSAGASHSVALLTGDSVCSWGRGEDGQLGHGDADERHLPTI  59
                                                        *

AtUVR8     61 LSALDGHQIVSVTCGADHTVAYSQSGMEVYSWGWGDFGRLGHGNSSDLFTPLPIKALHGI 120
MpUVR8.1   60 ISTLGECEISAITCGADHTTAYADSTRTVYSWGWGDFGRLGHGNSSDLFIPHPIKALRGI 119
MpUVR8.2   60 ISTLGECEISAITCGADHTTAYADSTRTVYSWGWGDFGRLGHGNSSDLFIPHPIKALRGI 119
                                                 *  * *           *

AtUVR8    121 RIKQIACGDSHCLAVTMEGEVQSWGRNQNGQLGLGDTEDSLVPQKIQAFEGIRIKMVAAG 180
MpUVR8.1  120 EISQIACGDSHCLAITTQGDVHSWGRNQNGQLGLGHNEDSLVPKKVVAFEGIAVKMLAAG 179
MpUVR8.2  120 EISQIACGDSHCLAITTQGDVHSWGRNQNGQLGLGHNEDSLVPKKVVAFEGIAVKMLAAG 179
                                        *

AtUVR8    181 AEHTAAVTEDGDLYGWGWGRYGNLGLGDRTDRLVPERVTSTGGEKMSMVACGWRHTISVS 240
MpUVR8.1  180 AEHTAAVTESGKLYGWGWGRYGNLGLGDRNDRLVPAEVAGVNNEKFTLVACGWRHTIAVA 239
MpUVR8.2  180 AEHTAAVTESGKLYGWGWGRYGNLGLGDRNDRLVPAEVAGVNNEKFTLVACGWRHTIAVA 239
                                 *  *                                *

AtUVR8    241 YSGALYTYGWSKYGQLGHGDLEDHLIPHKLEALSNSFISQISGGWRHTMALTSDGKLYGW 300
MpUVR8.1  240 ESGNLYTFGWSKYGQLGHGDYLDHLVPHQVAALKNNPIVQISGGWRHTVALDSSGRLYGW 299
MpUVR8.2  240 ESGNLYTFGWSKYGQLGHGDYLDHLVPHQVAALKNNPIVQISGGWRHTVALDSSGRLYGW 299
                        *                                   *               *

AtUVR8    301 GWNKFGQVGVGNNLDQCSPVQVRFPDDQKVVQVSCGWRHTLAVTERNNVFAWGRGTNGQL 360
MpUVR8.1  300 GWNKFGQVGVGNTDDQTSPQLVKNLAEEKVKQVSCGWRHTVCITERGNVFSWGRGTSGQL 359
MpUVR8.2  300 GWNKFGQVGVGNTDDQTSPQLVKNLAEEKVKQVSCGWRHTVCITERGNVFSWGRGTSGQL 359
                *                                   *               *

AtUVR8    361 GIGESVDRNFPKIIEALSVDGASGQHIESSNIDPSSGKSWVSPAERYAVVPDET------ 414
MpUVR8.1  360 GHGDAVDRSLPKRIEALSADGLACQELESSRTTTSTGSHWISPSERYAVVPVETVRSLSR 419
MpUVR8.2  360 GHGDAVDRSLPKRIEALSADGLACQELESSRTTTSTGSHWISPSERYAVVPVET------ 413
                                                        *

AtUVR8    415 ----GLTDGSSKGNGGDISVPQTDVKRVRI--                              440
MpUVR8.1  420 NMHQNANVGDNEVPSSDASVPDTDVKRLRTGF                              451
MpUVR8.2  414 -------VGDNEVPSSDASVPDTDVKRLRTGF                              438
```

Figure S1. Alignment of Marchantia MpUVR8.1 and MpUVR8.2 with Arabidopsis AtUVR8. Red asterisks (*) highlight conserved tryptophan (W) amino acid residues, including the AtUVR8 key triad tryptophans W233 (W232 in MpUVR8), W285 (W284 in MpUVR8), and W337 (W336 in MpUVR8), within their conserved GWRHT sequence motif. Green asterisks (*) highlight AtUVR8 aspartates D96 (D95 in MpUVR8) and D107 (D106 in MpUVR8).

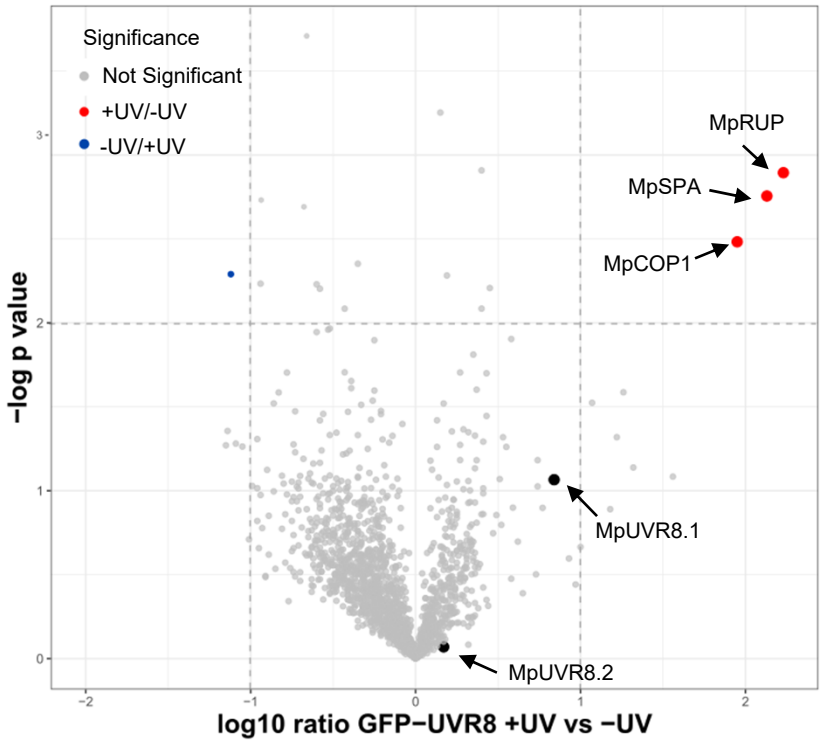

Figure S2. Volcano plot of GFP-MpUVR8 AP-MS under +UV versus -UV conditions. AP–MS was performed using a Marchantia *Pro*$_{MpUVR8}$*:GFP-*Mp*UVR8* (genomic) transgenic line grown for 7 days under continuous white light (50 µmol m^{-2} s^{-1}) without UV-B, or under continuous white light supplemented with narrowband UV-B (1.5 µmol m^{-2} s^{-1}) followed by a 20 min broadband UV-B exposure (25 µmol m^{-2} s^{-2}). Significantly enriched proteins were identified using a p-value cutoff of < 0.01 and a log10 fold change threshold of ±1.0. Grey dots represent non-significant proteins; red dots indicate proteins significantly enriched in +UV compared to –UV; blue dots indicate proteins significantly enriched in –UV compared to +UV. Arrows highlight proteins of interest.

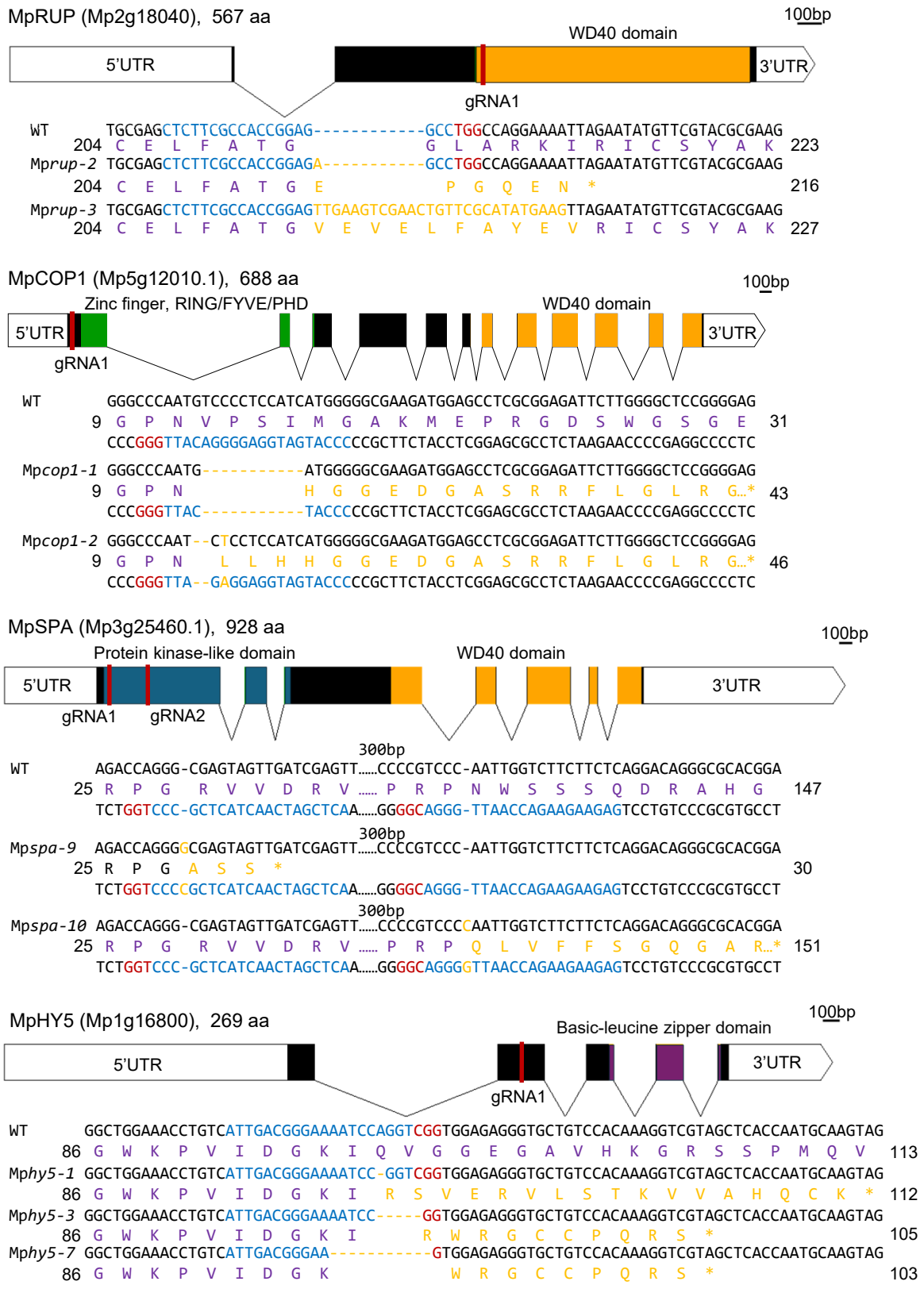

Figure S3. Gene structure and indication of the mutated sites in the corresponding mutants generated by CRISPR/Cas9. Untranslated (5' and 3' UTRs) and coding sequences are highlighted as white and colored boxes, respectively, with specific domains indicated. Introns are represented by lines connecting exons. The positions of the guide RNA (gRNA) (red bar, sequence in blue), protospacer adjacent motif (PAM) sequences (sequence in red), different mutations including resulting amino acid changes (in yellow), translated amino acids of wild-type (in purple) and the number of translated amino acids are also highlighted. The Mp*rup-2* mutant exhibits an insertion of one adenine (A) nucleotide, while Mp*rup-3* displays 27-bp insertion with a 15-bp deletion of endogenous sequence. Mp*cop1-1* and Mp*cop1-2* mutants show an 11-bp deletion and a 2-bp deletion with one cytosine (C) nucleotide substituted by thymine (T), respectively. Mp*spa-9* has an insertion of one guanine (G) nucleotide for gRNA1, whereas Mp*spa-10* exhibits an insertion of one cytosine (C) nucleotide for gRNA2. The Mp*hy5-1* mutant displays a deletion of one adenine (A) nucleotide, whereas Mp*hy5-3* and Mp*hy5-7* mutants show a 5-bp deletion and 11-bp deletion, respectively. All these mutations, except for Mp*rup-3*, result in a frameshift and early STOP codon in the coding sequence.

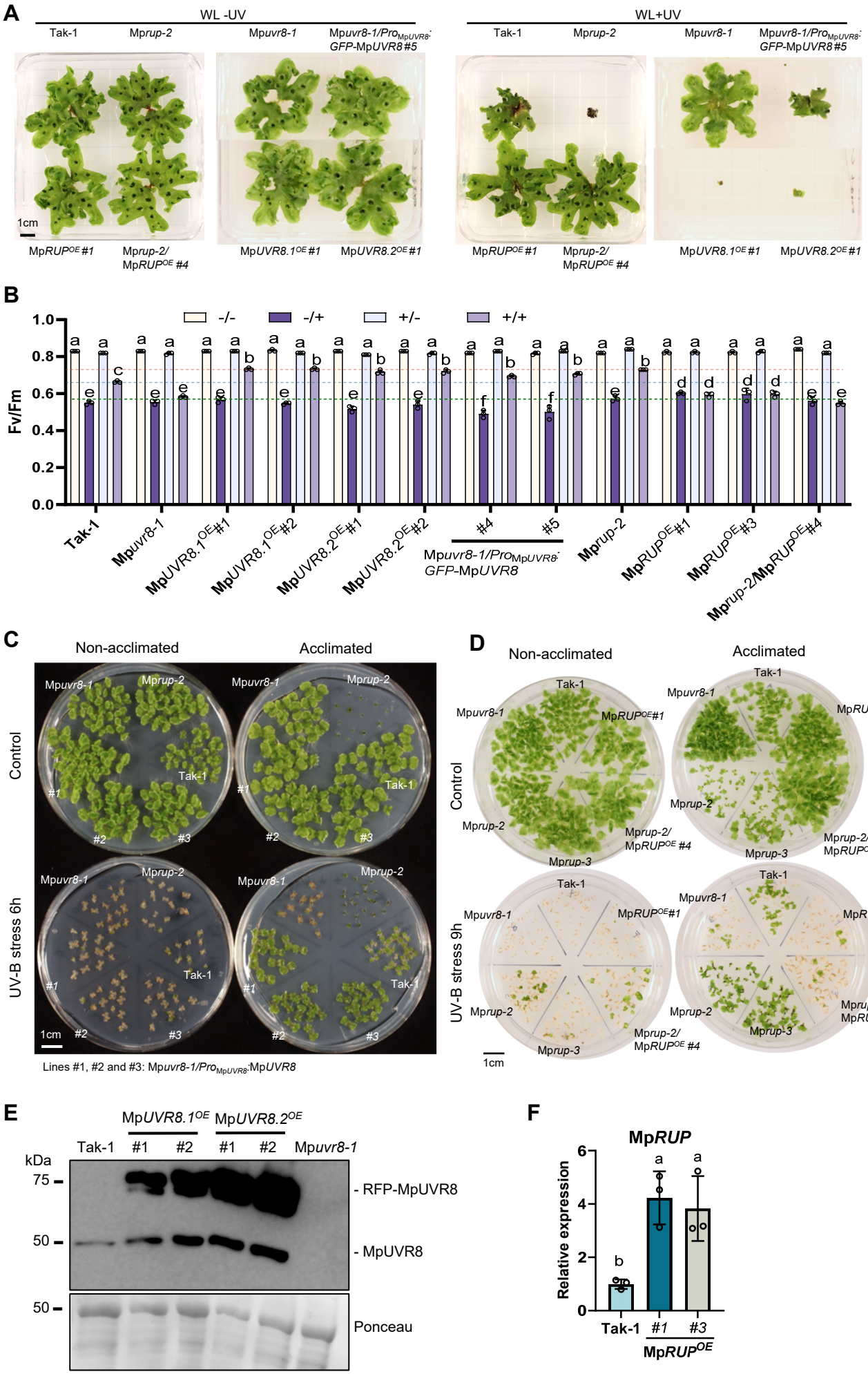

Figure S4. UV-B photomorphogenesis and photoprotection in MpUVR8 and MpRUP transgenic lines.

Figure S4. UV-B photomorphogenesis and photoprotection in MpUVR8 and MpRUP transgenic lines. **A)** Growth phenotype of 4-week-old wild-type (Tak-1), Mp*rup-2*, Mp*uvr8-1*, Mp*uvr8-1/Pro*$_{MpUVR8}$*:GFP*-Mp*UVR8* line *#5,* Mp*RUP*^{OE} *#1*, Mp*rup-2/*Mp*RUP*^{OE} *#4*, Mp*UVR8.1*^{OE} *#1*, and Mp*UVR8.2*^{OE} *#1* plants grown in white light supplemented (WL +UV) or not (WL -UV) with UV-B. Bar = 1 cm. **B)** F_v/F_m measurements in wild-type (Tak-1), Mp*uvr8-1*, Mp*UVR8.1*^{OE} lines *#1* and *#2*, Mp*UVR8.2*^{OE} *#1* and *#2*, Mp*uvr8-1/Pro*$_{MpUVR8}$*:GFP*-Mp*UVR8 #4* and *#5,* Mp*rup-2*, Mp*RUP*^{OE} *#1* and *#3*, and Mp*rup-2/*Mp*RUP*^{OE} *#4* grown for 7 days in white light (non-acclimated) or white light supplemented with UV-B (acclimated), without (non-stressed) or with (stressed) additional exposure to broadband UV-B stress for 60 min. -/-, non-acclimated, non-stressed; -/+, non-acclimated, stressed; +/-, acclimated, non-stressed; +/+, acclimated, stressed. Individual data points of biological replicates and means ± SD are shown (n = 3). Dashed horizontal lines indicate levels corresponding to acclimated and stressed Tak-1 (blue), Mp*uvr8-1* (green), and Mp*rup-2* (orange) plants. Different letters indicate statistically significant differences between the means ($P < 0.01$) as determined by two-way ANOVA followed by Tukey's post hoc honestly significant difference (HSD) test. **C** and **D)** UV-B stress tolerance of indicated plant genotypes grown for 7 days in white light supplemented (acclimated) or not (non-acclimated) with UV-B, then exposed or not to 6 hours of broadband UV-B. Pictures were taken after recovery for another 7 days in white light. Bar = 1 cm. (C) #1, #2 and #3: three independent Mp*uvr8-1/Pro*$_{MpUVR8}$:Mp*UVR8* lines. **E)** Immunoblot analysis of MpUVR8 and RFP-MpUVR8 levels in 14-day-old Tak-1, Mp*UVR8.1*^{OE}*#1*, Mp*UVR8.1*^{OE}*#2*, Mp*UVR8.2*^{OE}*#1*, Mp*UVR8.2*^{OE}*#2*, and Mp*uvr8-1* thallus. Ponceau staining is shown as loading control. Mp*UVR8.1*^{OE} = Tak-1/*Pro*$_{MpEF1\alpha}$:RFP-UVR8.1; Mp*UVR8.2*^{OE} = Tak-1/*Pro*$_{MpEF1\alpha}$:RFP-UVR8.2. **F)** RT-qPCR analysis of Mp*RUP* expression level in 14-day-old Tak-1 and two Mp*RUP*^{OE} lines. Individual data points of biological replicates and means ± SD are shown (n = 3). Different letters indicate statistically significant differences between the means ($P < 0.05$) as determined by one-way ANOVA followed by Tukey's post hoc honestly significant difference (HSD) test.

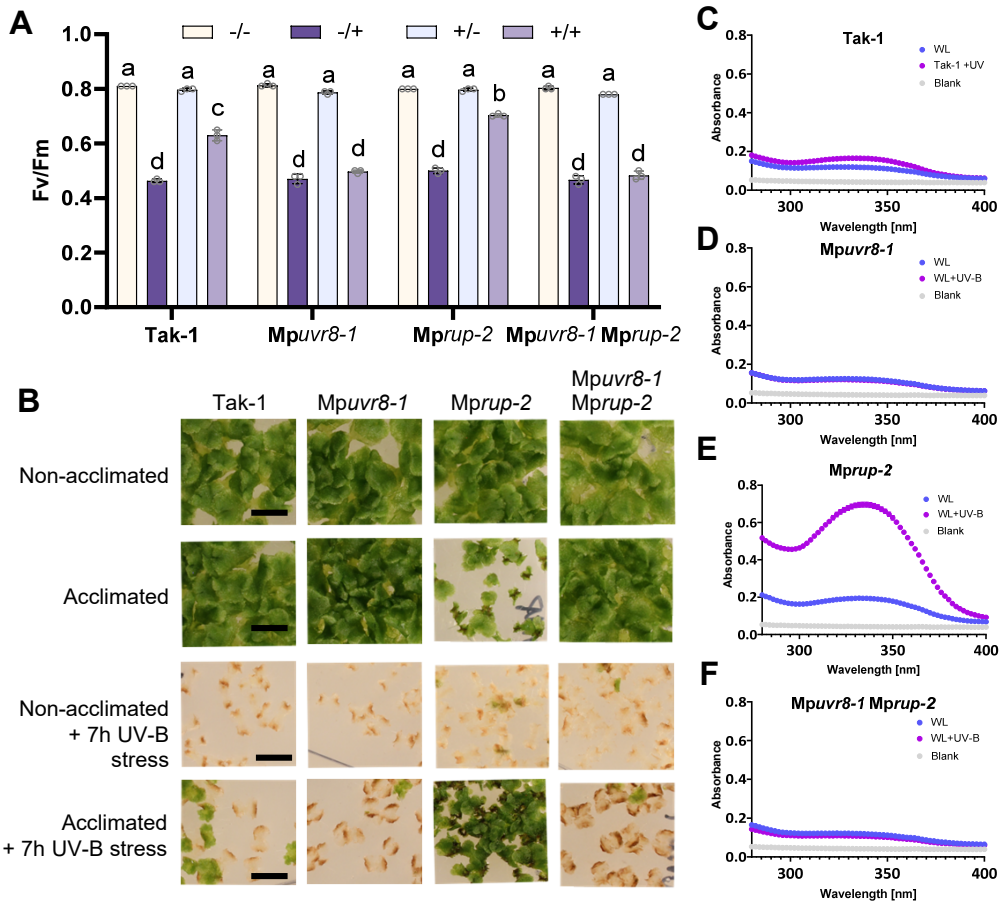

Figure S5. Enhanced photoprotection and UV-B-absorbing capacity of Mp*rup* depends on MpUVR8. **A)** F_v/F_m measurements in wild-type (Tak-1), Mp*uvr8-1*, Mp*rup-2*, and Mp*uvr8-1* Mp*rup-2* grown for 7 days in white light (non-acclimated) or white light supplemented with UV-B (acclimated), without (non-stressed) or with (stressed) additional exposure to broadband UV-B stress for 60 min. -/-, non-acclimated, non-stressed; -/+, non-acclimated, stressed; +/-, acclimated, non-stressed; +/+, acclimated, stressed. Individual data points of biological replicates and means ± SD are shown (*n* = 3). Different letters indicate statistically significant differences between the means (P < 0.01) as determined by two-way ANOVA followed by Tukey's post hoc honestly significant difference (HSD) test. **B)** UV-B stress resistance in Tak-1, Mp*uvr8-1*, Mp*rup-2*, and Mp*uvr8-1* Mp*rup-2* plants grown for 7 days in white light supplemented (acclimated) or not (non-acclimated) with UV-B, then exposed or not to 7 hours of broadband UV-B. Pictures were taken after recovery for another 7 days in white light. Bars = 1 cm. **C-F)** Absorbance spectra (280–400 nm) of methanolic extracts from 9-day-old Tak-1 (C), Mp*uvr8-1* (D), Mp*rup-2* (E), and Mp*uvr8-1* Mp*rup-2* (F) gemmalings grown for 7 days in white light and exposed (WL+UV-B, purple lines) or not (WL, blue lines) to supplemental UV-B (1.5 µmol m^{-2} s^{-1}) for 2 days. The gray line shows the absorbance of the buffer (blank). Values of independent measurements and means ± SEM are shown (*n* = 3).

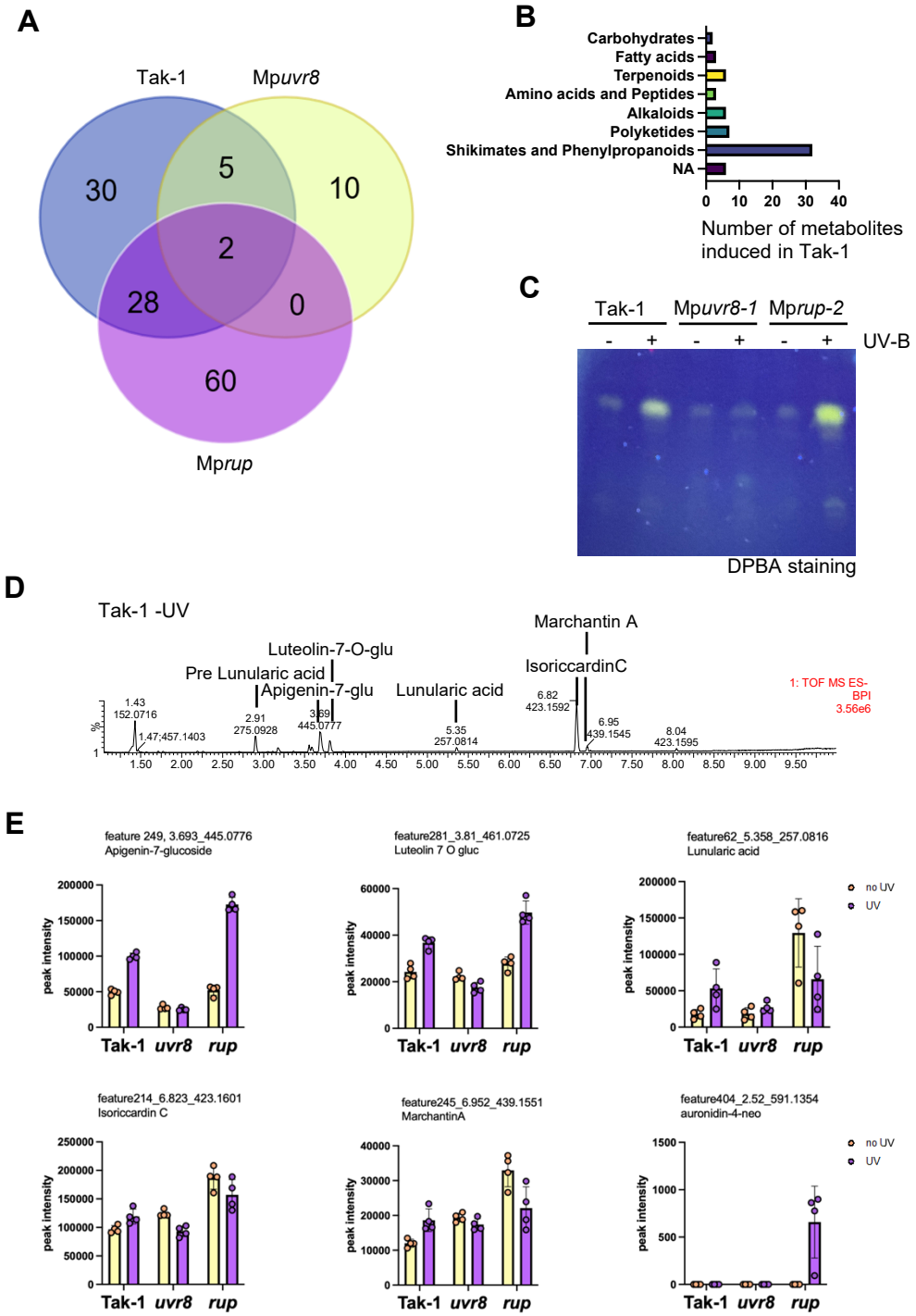

Figure S6. MpUVR8- dependent regulation of metabolite accumulation upon UV-B exposure. **A)** Venn diagram showing overlaps between upregulated metabolites (FC> or =1.5, p-adj < or =0.05) upon exposure to 2 days UV-B in 9-day-old wild-type (Tak-1), Mp*uvr8-1* (Mp*uvr8*), and Mp*rup-2* (Mp*rup*) gemmalings. **B)** Distribution of the number of compounds induced under UV-B in wild type (FC> or =1.5, p-adj < or =0.05), according to their chemical classes. Corresponding metabolite lists: table S7. **C)** High-performance thin-layer chromatography (HPTLC) analysis of flavonol glycoside levels in 7-d-old gemmalings of wild type (Tak-1), Mp*uvr8-1*, and Mp*rup-2* grown for 7 days in white light and exposed, or not, to supplemental UV-B for 2 days. DPBA, diphenylboric acid 2-aminoethylester. **D** and **E)** Metabolomic analysis of 9-day-old plants of Tak-1, Mp*uvr8-1*, and Mp*rup-2* grown for 7 days in white light and exposed (+) or not (-) to supplemental UV-B (1.5 µmol m^{-2} s^{-1}) for 2 days (n = 5, 12 plants per replicate). (D) UHPLC-MS chromatogram from -UV-B Tak-1 sample. Metabolites corresponding to major peaks are annotated based on their accurate mass and MS2 spectra. (E) Relative quantifications of selected compounds in Tak-1, Mp*uvr8-1* (*uvr8*), and Mp*rup-2* (*rup*) methanolic extracts from plants exposed to UV-B (purple, right bar, UV) or not (yellow, left bar, no UV). Individual data points of biological replicates and means ± SD are shown (n = 4).

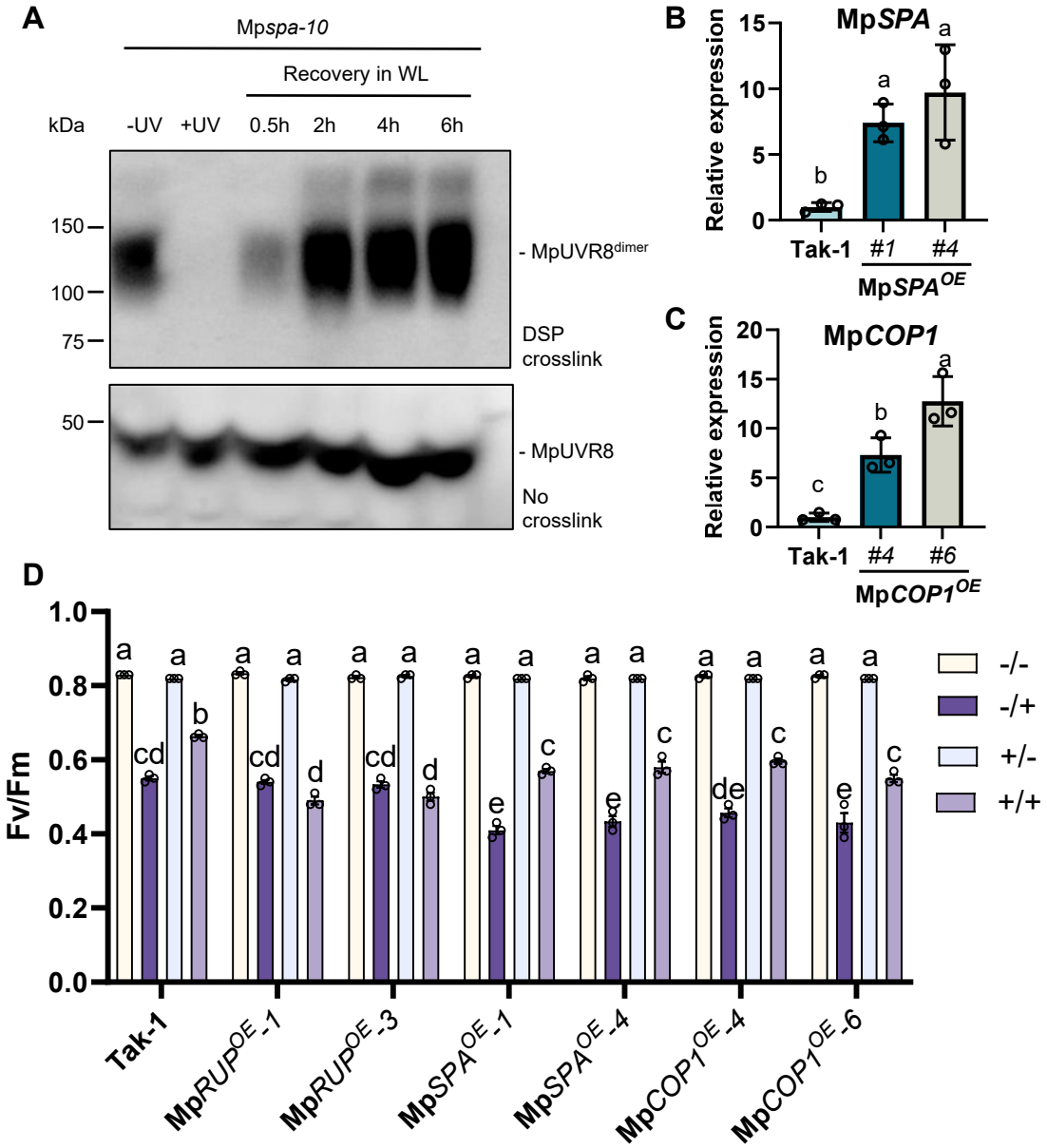

Figure S7. MpSPA does not affect MpUVR8 redimerization, but MpCOP1 and MpSPA overexpression reduces basal UV-B tolerance. **A)** Immunoblot analysis of MpUVR8 levels in 7-day-old Mp*spa-10* gemmalings irradiated for 20 min with broadband UV-B before recovery in white light (WL) for the indicated times. Top: MpUVR8 dimer levels in DSP-crosslinked protein extracts. Bottom: total MpUVR8 levels in non-crosslinked extracts. **B)** RT-qPCR analysis of Mp*SPA* expression level in 14-day-old plants of Tak-1 and Mp*SPA*^{OE} lines *#1* and *#4*. Individual data points of biological replicates and means ± SD are shown (n = 3). Letters indicate statistically significant differences between the means (P < 0.05) as determined by one-way ANOVA followed by Tukey's post hoc honestly significant difference (HSD) test. **C)** RT-qPCR analysis of Mp*COP1* expression level in 14-day-old plants of Tak-1, Mp*COP1*^{OE} lines *#4* and *#6*. Individual data points of biological replicates and means ± SD are shown (n = 3). Letters indicate statistically significant differences between the means (P < 0.05) as determined by one-way ANOVA followed by Tukey's post hoc honestly significant difference (HSD) test. **D)** F_v/F_m measurements in wild-type (Tak-1), Mp*RUP*^{OE} lines *#1* and *#3*, Mp*SPA*^{OE} *#1* and *#4*, and Mp*COP1*^{OE} *#4* and *#6* grown for 7 days in white light (non-acclimated) or white light supplemented with UV-B (acclimated), without (not stressed) or with (stressed) additional exposure to broadband UV-B stress for 60 min. -/-, not acclimated, not stressed; -/+, not acclimated, stressed; +/-, acclimated, not stressed; +/+, acclimated, stressed. Individual data points of biological replicates and means ± SD are shown (n = 3). Letters indicate statistically significant differences between the means (P < 0.01) as determined by two-way ANOVA followed by Tukey's post hoc honestly significant difference (HSD) test.

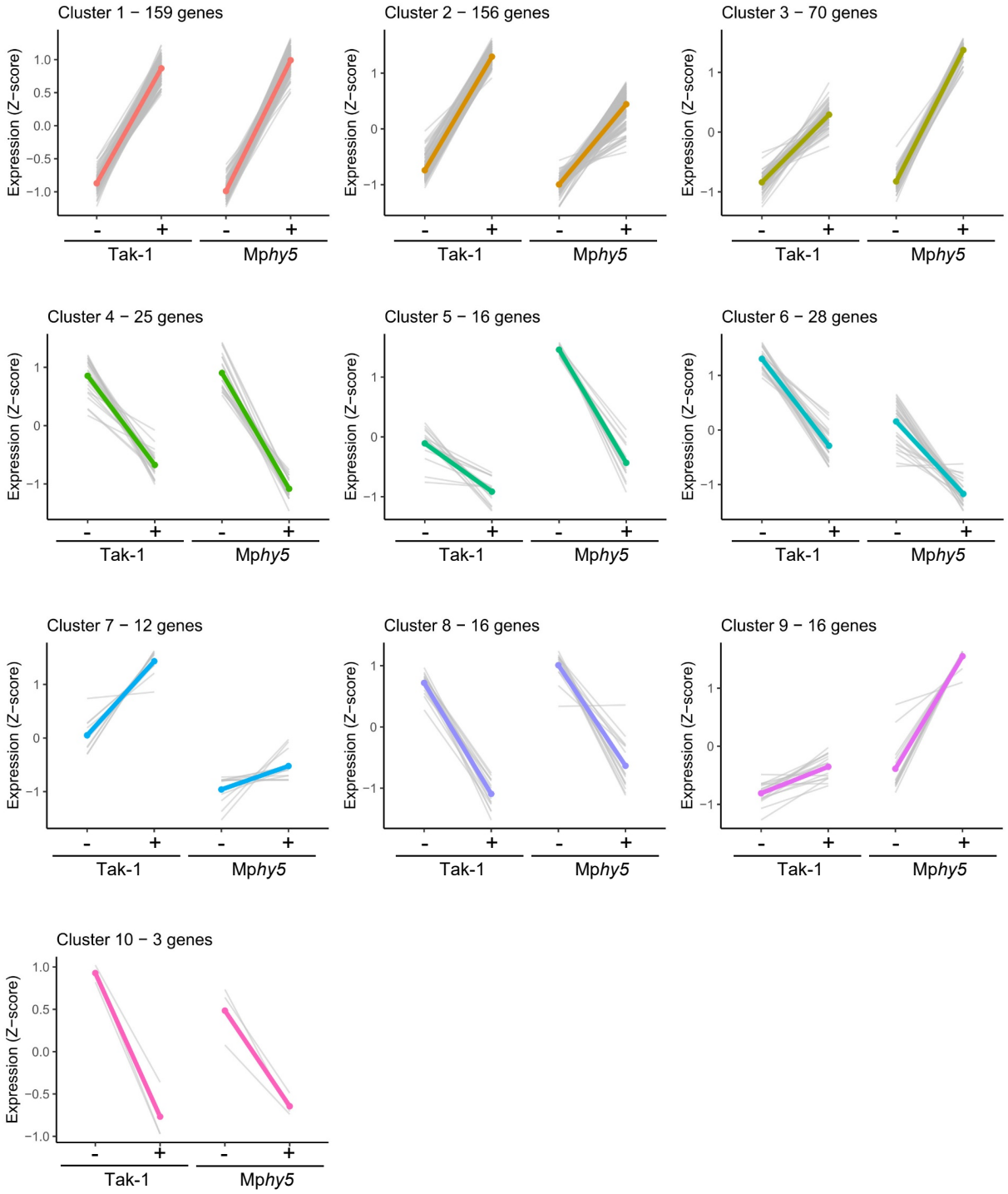

Figure S8. MpHY5 plays a minor role in the regulation of UV-B-induced gene expression changes. Gene expression profiles in clusters identified by hierarchical clustering. Z-scores for normalized read count values for each gene (gray lines) and for the cluster average (colored line) are shown.

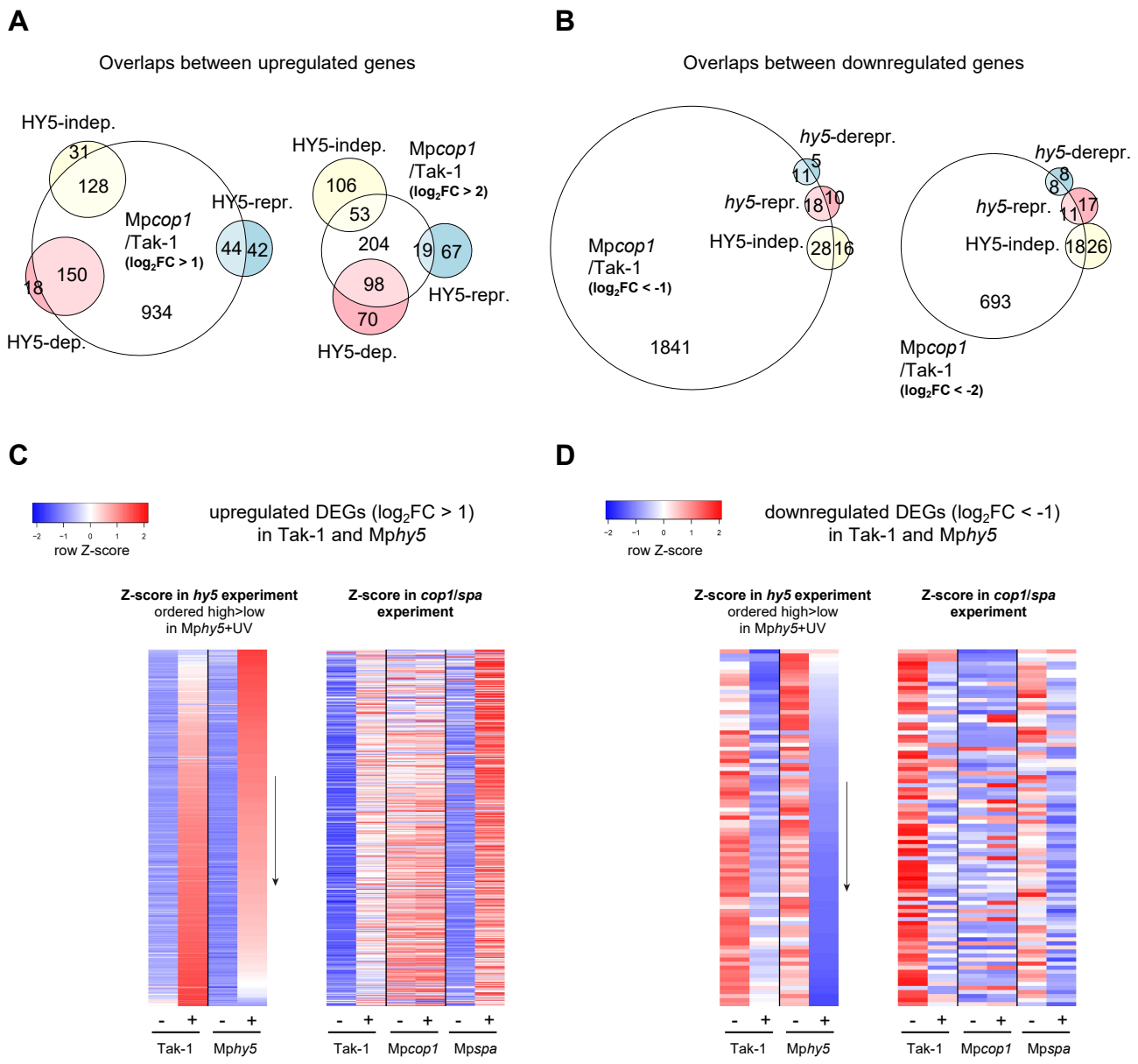

Figure S9. MpHY5 and MpCOP1 regulate UV-B-induced gene expression in an antagonist manner. **A)** Euler plots showing overlaps between upregulated DEGs (p-adj < 0.05) in Mp*cop1*/Tak-1 in white light (left: $\log_2$FC > 1; right: $\log_2$FC > 2) and genes that are induced after 3h of UV-B. UV-B-upregulated genes are separated into 3 categories: genes that are induced in a MpHY5-independent manner ("HY5-indep.", fig. S7 cluster 1), genes that are dependent on MpHY5 for their full induction or hypoinduced in Mp*hy5* ("HY5-dep.", fig. S7 clusters 2 and 7) and genes that are hyperinduced in Mp*hy5* or whose induction is repressed by HY5 ("HY5-repr.", fig. S7 clusters 3 and 9). Corresponding gene lists: table S8a. **B)** Euler plots showing overlaps between downregulated DEGs (p-adj < 0.05) in Mp*cop1*/Tak-1 in white light (left: $\log_2$FC < -1; right: $\log_2$FC < -2) and genes that are repressed after 3h of UV-B. UV-B-downregulated genes are separated into 3 categories: genes that are repressed in a MpHY5-independent manner ("HY5-indep.", fig. S7 clusters 4, 8 and 10), genes that are somewhat constitutively repressed in Mp*hy5* ("*hy5*-repr.", fig. S7 cluster 6) and genes that are derepressed in white light-grown Mp*hy5* ("*hy5*-derepr.", fig. S7 cluster 5). Corresponding gene lists: table S8b. **C)** Heatmap of all genes upregulated ($\log_2$FC > 1 and p-adj < 0.05) by UV-B in Tak-1 and/or Mp*hy5*. Red and blue colors indicate normalized read count Z-scores in RNA-seq experiments including Tak-1 and Mp*hy5* (left) and Tak-1, Mp*cop1* and Mp*spa* (right). Z-scores were calculated separately for the two experiments and genes were ordered in a decreasing order according to the Z-score in Mp*hy5*+UV (arrow). **D)** Heatmap of all genes downregulated ($\log_2$FC < -1 and p-adj < 0.05) by UV-B in Tak-1 and/or Mp*hy5*. Red and blue colors indicate normalized read count Z-scores in RNA-seq experiments including Tak-1 and Mp*hy5* (left) and Tak-1, Mp*cop1* and Mp*spa* (right). Z-scores were calculated separately for the two experiments and genes were ordered in a decreasing order according to the Z-score in Mp*hy5*+UV (arrow).

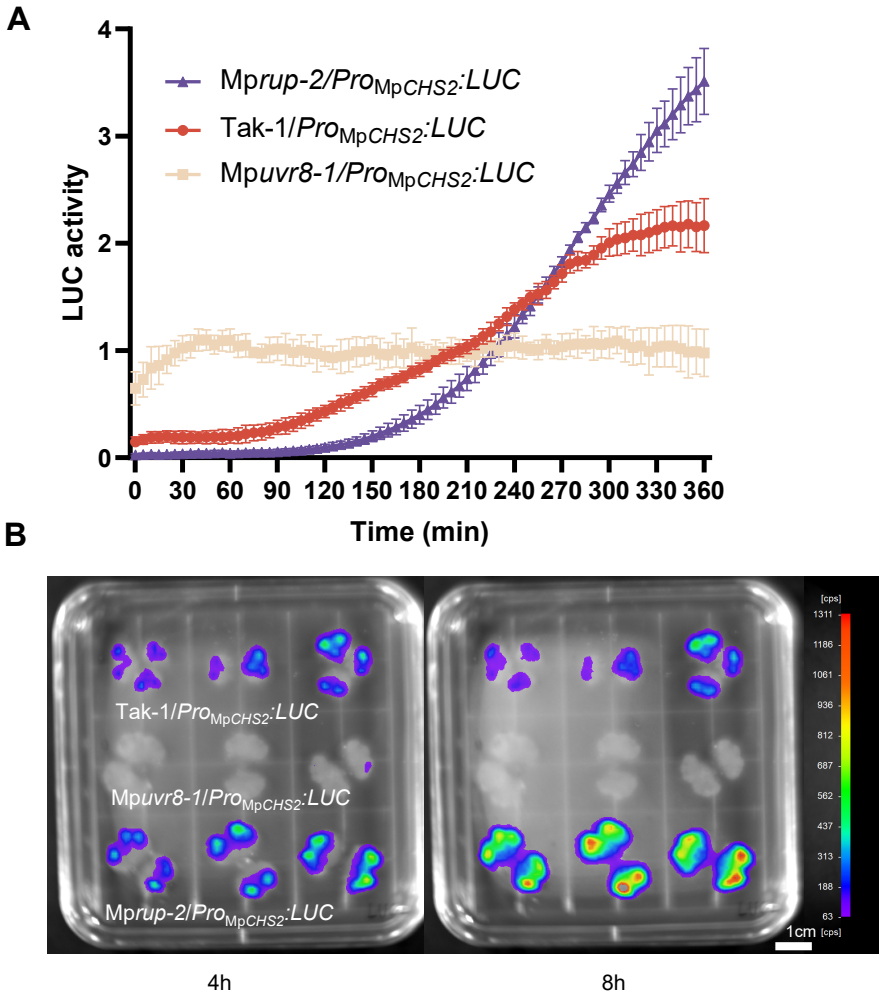

Figure S10. LUC activity of a *Pro*$_{\text{Mp}CHS2}$*:LUC* reporter in Tak-1, Mp*uvr8-1*, and Mp*rup-2* backgrounds upon UV-B exposure. **A)** The counts per second (cps) of luciferase (LUC) activity were normalized to average expression level measured in 3-day-old gemmalings of the following lines: Tak-1/*Pro*$_{\text{Mp}CHS2}$*:LUC*, Mp*uvr8-1*/*Pro*$_{\text{Mp}CHS2}$*:LUC*, and Mp*rup-2*/*Pro*$_{\text{Mp}CHS2}$*:LUC.* These gemmalings were grown in 96-well plates under white light, and pre-sprayed with luciferin 24 h before a 20-min exposure to broadband UV-B. The LUC activity was monitored for up to 360 min after the UV-B induction. Values of independent measurements and means ± SD are shown (n = 8). **B)** Analysis of LUC activity in 14-day-old thalli of Tak-1/*Pro*$_{\text{Mp}CHS2}$*:LUC*, Mp*uvr8-1*/*Pro*$_{\text{Mp}CHS2}$*:LUC*, and Mp*rup-2*/*Pro*$_{\text{Mp}CHS2}$*:LUC* lines followed by 20 min of broadband UV-B exposure at 4 h (left) and 8 h (right).